PERGAMON

International Journal of Multiphase Flow 26 (2000) 1141–1181

International Journal of Multiphase Flow

www.elsevier.com/locate/ijmulflow

On bubbles rising in line

M.C. Ruzicka

Institute of Chemical Process Fundamentals, Czech Academy of Sciences, Rozvojova 135, Prague 16502, Czech Republic

Received 18 October 1998; received in revised form 28 June 1999

Abstract

The dynamic behaviour of equal-sized spherical gas bubbles rising in vertical line was studied numerically at Reynolds number (*Re*) 50–200. A force-law model was suggested for hydrodynamic interactions within the bubble chain. Three forces acted on each bubble: buoyancy, viscous drag, and inviscid inertia forces. Both local (nearest-neighbour approximation) and non-local (distant effects) interactions between bubbles were considered. The viscous non-local interactions consisted in creation of velocity disturbances by the passage of bubbles and resulted in progressive drag reduction down the chain. Due to the balance between creation and decay of the disturbances, the distant interactions affected only a certain number of the anterior bubbles until the limit chain drag was reached. This drag then applied to all remaining bubbles independent of their positions and the distant effects were thus eliminated. The inviscid non-local interactions consisting in inertial coupling between distant bubbles were found weaker than the viscous non-local interactions and were, therefore, neglected. Two kinds of bubble chain with different boundary conditions were distinguished: the free-end chain and the fixed-end chain. The free-end chain tended to split into smaller bubble groups that subsequently interacted and produced a highly fragmented long-time chain structure. The typical phenomena in bubble interactions were the following: merger, separation, pairing-off, re-pairing, and oscillation. The fixed-end chain allowed for uniform spacing, rose faster than an isolated bubble, and supported propagation of concentration disturbances. Uniform spacing became unstable at low *Re* and bubbles displayed chaotic behaviour. The results produced by the model were compared with data published in the literature. The model was able to predict and explain the key phenomena observed in experiments. This correspondence was obtained in the nearest-neighbour approximation (the distant effects may not be very strong in real systems). Intensive non-local interactions affected the chain behaviour substantially. The analogy between hydrodynamic and mechanical 'masses-on-spring' systems was pointed out.

E-mail address: ruzicka@icpf.cas.cz (M.C. Ruzicka).

0301-9322/00/$ - see front matter
PII: S0301-9322(99)00078-6

Keywords: Bubble chain; Hydrodynamic interactions; Viscous coupling; Inertial coupling; Distant effects; Dynamic behaviour

1. Introduction

The results on hydrodynamic interactions of particles arranged in a one-dimensional array found in the literature are presented here. In many ways, these arrays display similar features of behaviour regardless of the physical nature of the particles (bubbles, drops, and solids).

1.1. Two bubbles

Low Reynolds number behaviour of two particles has been studied thoroughly for a long time (Happel and Brenner, 1965; Rushton and Davies, 1978). In absence of inertial effects, the particles move with constant and equal velocities and are separated by a constant spacing. The pair is always faster than an isolated particle, and the total pair drag decreases with decreasing particle spacing.

High Reynolds number analysis consists in finding the potential with two spherical boundary conditions (see e.g. Kok, 1993a for discussion). The inviscid interaction force is an inertial repulsive force rapidly decaying with distance (Lamb, 1932; Harper, 1970). The equations of motion for two bubbles (in general position) were derived by Biesheuvel and van Wijngaarden (1982). Vertically aligned bubbles repel each other and separate unlimitedly.

For *intermediate Reynolds number* $Re \sim 10^2$, the equations of motion for two bubbles (in general position) were derived by Kok (1993a, 1993b), Kumaran and Koch (1993a, 1993b). In their approximation, both particles experienced the same drag and the pair basically followed the inviscid scenario (van Wijngaarden, 1993). The full Navier–Stokes equation was solved numerically by Yuan and Prosperetti (1994, referred to as YP), and the true drag coefficients of both bubbles were calculated. The leading drag was almost unaffected and equal to the isolated bubble drag. The trailing drag was reduced substantially by the shielding effect of the preceding bubble: the lower the spacing, the higher the drag reduction. A stable bubble pair with an equilibrium spacing was predicted. Harper (1997, referred to as H97), suggested a general approach for calculations of drag force on bubbles rising in line, and his result for two bubbles agreed well with that of YP. The drop in the trailing particle drag and no effect on the leading particle drag were confirmed by experiments (Lee, 1979; Tsuji et al., 1982; Temkin and Ecker, 1989; Zhu et al., 1994) and simulations (Sirignano, 1993).

1.2. More bubbles

Low Reynolds number steady flow past a line of particles fixed in space was studied theoretically (Wang and Skalak, 1969; Leichtberg et al., 1976b; Ganatos et al., 1978; Pruppacher and Klett, 1978; Harper, 1983). The drag depended on the particle position in the chain was minimum in the middle, increased symmetrically toward both ends (Leichtberg et al.,

1976b; Ganatos et al., 1978), and decreased with increasing chain length and decreasing particle spacing. Dynamic behaviour of three freely moving particles was studied experimentally (Happel and Pfeffer, 1960) and re-pairing was observed. Leichtberg et al. (1976a) performed a detail dynamic study of chains with 3–25 rigid particles. Pairing-off was observed at the front end and particles were gradually lost from the rear end. The split pairs interacted in a complex way and produced a highly fragmented final structure of the chain. Pairing-off for bubble chains was predicted on theoretical grounds (Morrison, 1973; Harper, 1983; Lerner and Harper, 1991;) and observed experimentally (Katz and Meneveau, 1996, referred to as KM).

In *high Reynolds number* limit, the Harper's (Harper, 1970) two-bubble result also applies to more bubbles; the interactive force has only the repulsive component. The potential was calculated for groups of several spheres (Helfinstine and Dalton, 1974) and infinite row of spheres (Michael, 1965).

In *intermediate Reynolds number* range, our knowledge about the chain behaviour is only superficial and very limited. No theory is available, except for the H97 approach. Experiments (Wang and Liu, 1992; Liang et al., 1996) and simulations (Tal et al., 1983; Tsai and Sterling, 1990; Ramachandran et al., 1991; Chiang and Sirignano, 1993) with three particles gave first results on the particle drag. The leading drag was close to the single particle value, and both trailing drags were roughly equal (for uniform spacing) and reduced, mainly at low particle spacing. Both trailing particles displayed similar wake structures. KM performed experiments on wake interactions between small and closely spaced bubbles in coalescent system at relatively low Re 0.2–35 and the pairing-off process was well documented. The bubbles in pairs coalesced instead of forming the equilibrium doublet predicted by YP for Re 50–200. The above cases refer to the situation in which a *finite* chain moves through a virtually *infinite* extent of fluid.

The situation when a virtually *infinite* continuously generated chain passes through a *finite* layer of fluid is qualitatively different. Continuously generated chains of bubbles were studied in numerous experiments (Poutanen and Johnson, 1959; Crabtree and Bridgwater, 1969; Marks, 1973; Omran and Foster, 1977; Martin and Chandler, 1982; Li et al., 1997b, 1998). These chains allowed for uniform spacing, rose faster than an isolated particle, and the chain drag decreased with decreasing bubble spacing. The uniform spacing became unstable at low Re and bubbles started to oscillate in a irregular way — chaos (Nguyen et al., 1996; Li et al., 1997a). Chaotic behaviour was also observed at the bubbles formation at the orifice (Tritton and Egdell, 1993; Mittoni et al., 1995; Drahoš et al., 1997) and explained by dynamic coupling between the gas and liquid phases (Ruzicka et al., 1997).

It follows that we lack knowledge about detail dynamic behaviour of particles in one-dimensional arrays at intermediate Re. Therefore, a simple modelling concept is suggested here that enables us to calculate positions and velocities of individual particles within the chain undergoing hydrodynamic interactions.

2. Model

Two kinds of bubble chain with different boundary conditions are distinguished here: the

free-end chain and the fixed-end chain, Fig. 1. In the *free-end chain*, the first and last particles miss one neighbour. This corresponds to a finite chain freely moving through unbounded fluid. The first (leading) particle obeys a different drag law than the remaining (trailing) particles. In the *fixed-end chain*, all particles are identical and trailing (interior) and have both neighbours. This correspond to either the experimental situation, where the particles are continuously supplied and pass through a finite layer of fluid (the chain is bounded by the nozzle from below and by the surface from above) or the theoretical model, where the chain under study represents a 'window' within a longer chain.

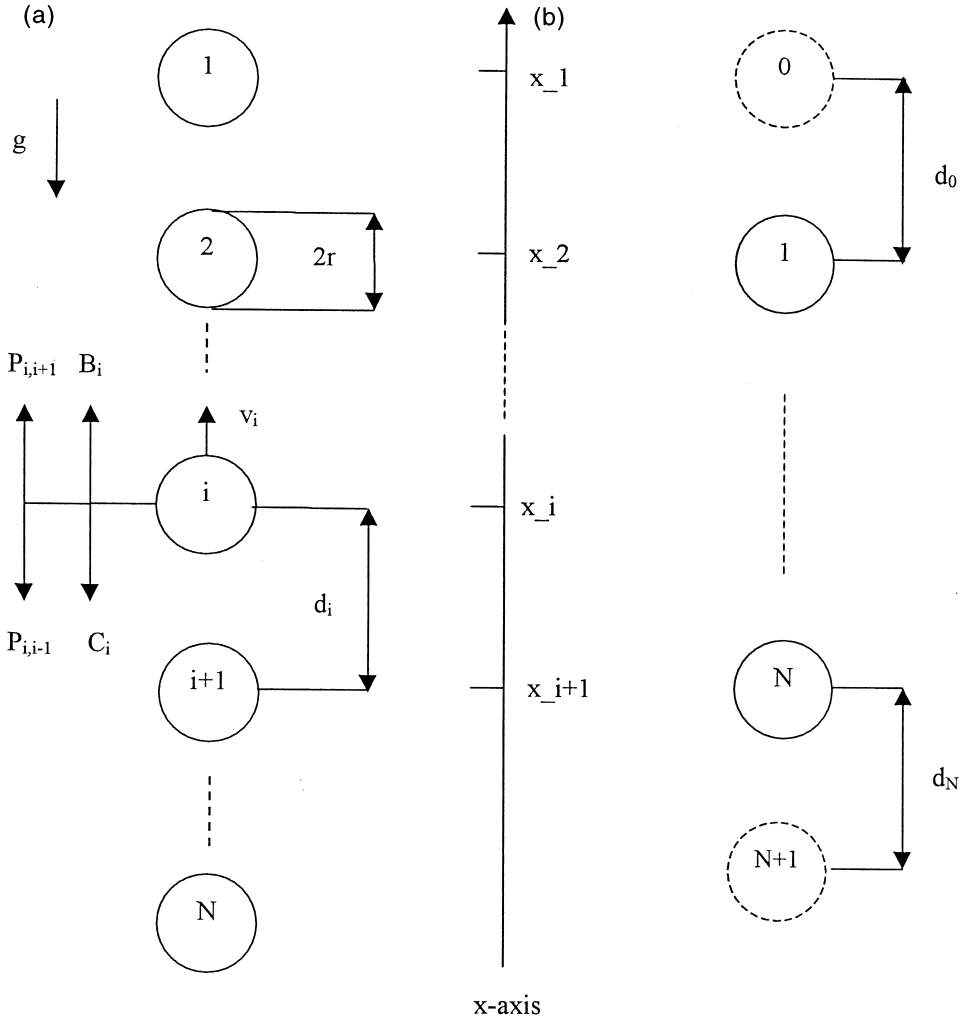

Fig. 1. Two different kinds of chain. (a) Free-end chain has no boundaries and the first and last particles miss one neighbour. (b) Fixed-end chain has two boundary particles 0 and $N+1$.

2.1. Local interactions of bubbles (nearest-neighbour approximation)

Let us consider spherical nondeformable incompressible equal-sized gas bubbles rising freely under buoyancy in a vertical line in an unbounded body of quiescent liquid, Fig. 1(a). Three forces are considered to act on each bubble: buoyancy, viscous drag, and inviscid inertia forces. The simplest case is considered first, where each bubble interacts only with the nearest neighbours on each side, *local interactions*. This approximation provides the basic pattern of chain behaviour. Effects coming from distant bubbles, *non-local interactions*, are explored next, as a correction to the local approximation.

2.1.1. Viscous force

The local viscous force equals the viscous component of the total pairwise interaction force found by the numerical solution of the Navier–Stokes equation by YP.

1. It is assumed that the first (leading) bubble has the same drag as the *first* bubble in YP, and all other (trailing) bubbles in the chain have the same drag as the *second* bubble in YP. In other words, independent of their position within the chain, all trailing bubbles follow the same drag law and are affected only by the nearest preceding wake. This assumption is realistic since both experiments (Wang and Liu, 1992; Liang et al., 1996) and numerical simulations (Tal et al., 1983; Ramachandran et al., 1991) on several particles in line show that the wake structure of all trailing particles are similar and the drag values are close. Additional support comes from long chains continuously generated in numerous experiments (see Section 1), where the particles kept uniform spacing; this would be impossible if each of them followed a different drag law depending on its position.
2. It is assumed that no viscous effect on a given bubble comes from the bubble behind it. This is a logical assumption since the viscous interactions between bubbles consist in creation of velocity disturbances and generation of vorticity that are experienced only by the downchain bubbles. This assumption is supported by the results of Ramachandran et al. (1991) and YP. The viscous interaction force is thus directed upwards drawing a bubble into the preceding wake.

Moore (1963) derived the expression for steady drag coefficient of a single bubble at intermediate Re,

$$C_0 = 48Re^{-1}(1 - F \cdot Re^{-0.5}), \tag{1}$$

where the drag factor F had a constant value $F \approx 2.2$. Reynolds number $Re = 2rv_0/\nu$ is based on single bubble velocity

$$v_0 = \left(\frac{8gr}{3C_0}\right)^{0.5}, \tag{2}$$

with bubble radius r, liquid kinematic viscosity ν, and gravity acceleration g. If we add the second bubble to form a vertically aligned pair, the value of F is no longer constant but depends on bubble position, bubble distance, and Re (YP). The following approximation formulas were suggested (see Appendix A) for the leading and trailing drag factors:

$$F_1(s) = 2.2 + 6\exp(1.2 - s) - 30\exp(2.4 - 2s), \quad \text{Leading bubble: 1} \tag{3}$$

$$F_2(s) = 2.2 + 2.5(s - 2)^{-0.6}, \quad \text{Trailing bubbles: 2, 3, \ldots, } N \tag{4}$$

where $s = d/r$ is the nondimensional centre-to-centre bubble distance and d is the dimensional one. The comparison of the Eqs. (3) and (4) with the original data is shown in Fig. 2. The drag force on bubble i rising with velocity v_i in liquid of density ρ is given by

$$D_i = \frac{1}{2}\rho v_i^2 \pi r^2 C_i, \tag{5}$$

where the viscous drag coefficient is given by

$$C_i = 48Re^{-1}\left(1 - F_i Re^{-0.5}\right) = C_{\mathrm{d}}. \tag{6}$$

The dimensional centre-to-centre distance between bubbles i and $i+1$ is denoted by $d_i = x_i - x_{i+1}$ (Fig. 1(a)) and $s_i = d_i/r$. The drag factors are given by

$$F_i = F_1(s_1) \quad \text{for } i = 1, F_i = F_2(s_{i-1}) \quad \text{for } i > 1. \qquad \text{(Nearest-neighbour approximation)} \tag{7}$$

Fig. 3 shows the leading and trailing drag coefficients versus bubble spacing for several Re. The leading drag almost coincides with the single bubble value and is always greater than the trailing drag. The leading bubble is, therefore, the slowest in the chain. The trailing drag is considerably reduced by the shielding effect of the preceding bubble (cyclists know this effect well). The limit single bubble value is approached slowly with increasing spacing, making the viscous force long-range. The values of both the coefficients C_1 and C_2 and their difference $C_1 - C_2$ decrease with increasing Re. The difference also decreases with increasing bubble spacing at fixed Re. Drag difference between *any two* neighbouring bubbles represents an

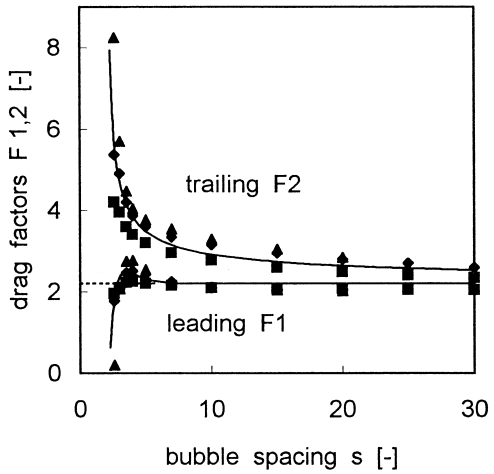

Fig. 2. Leading F_1 and trailing F_2 drag factors. Model (full lines); YP data (marks): $Re = 50$ (■), $Re = 100$ (◆), $Re = 200$ (▲); single bubble value $F = 2.2$ (dotted line).

effective attractive force between them. This leads to the formation of bubble clusters. The above facts are crucial for the chain behaviour.

It follows that the viscous component of the bubble–bubble interaction is a unidirectional long-range attracting force accelerating a bubble into the wake of the preceding bubble with intensity decreasing with increasing *Re*.

2.1.2. Inviscid force

The local inviscid (potential, inertial) force equals the inviscid component of the total pairwise interaction force found by YP. This force comes from the inertial effects of a body moving in fluid. The presence of the body induces a flow field that communicates pressure forces on other bodies (Lamb, 1932; Milne-Thomson, 1968). For a vertically aligned pair of equal bubbles, this force is symmetric, repulsive, and decaying rapidly with bubble spacing. This reflects the simple fact that the liquid entrapped in the gap between rising bubbles moves slowly and has higher pressure. The leading order term s^{-4} was found by several authors (Lamb, 1932; Harper, 1970; Biesheuvel and van Wijngaarden, 1982; Kok, 1993a, 1993b; Kumaran and Koch, 1993a, 1993b, YP).

The expression of the inviscid interaction force $P_{i,j}$, experienced by bubble i due to the presence of the neighbouring bubble $j = i \pm 1$, is given by (Lamb, 1932, Article 138, Eq. (4); Harper, 1970, Eq. (2.3):

$$P_{i,j} = \frac{1}{2}\rho v_j^2 \pi r^2 C_{i,j}, \tag{8}$$

where $C_{i,j}$ is the potential force coefficient

$$C_{i,j} = 12 s^{-4} = C_{\mathrm{p}}. \tag{9}$$

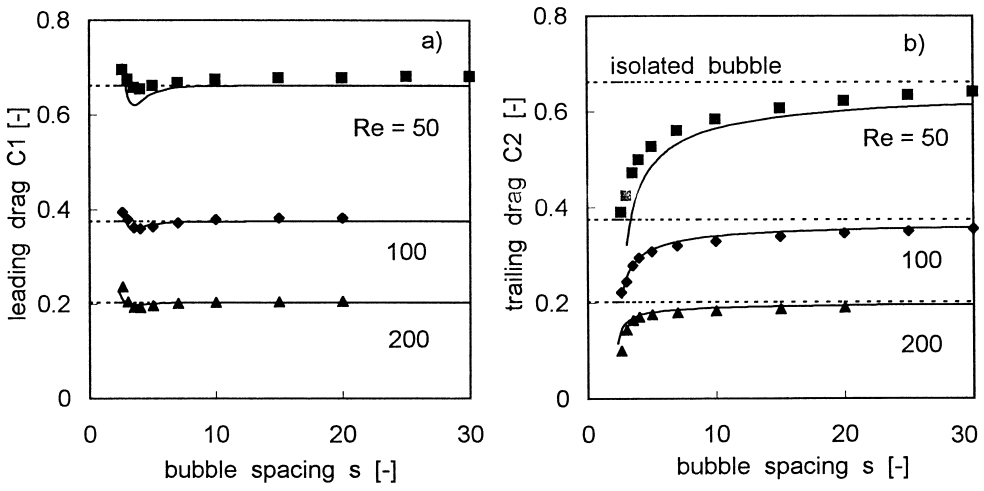

Fig. 3. (a) Leading C_1 and (b) trailing C_2 drag coefficients of bubbles in vertical pair. Model (full lines); YP data (marks): $Re = 50$ (■), $Re = 100$ (◆), $Re = 200$ (▲); single bubble drag (dotted lines).

The bubble spacing takes values $s = s_i$ for $j = i + 1$ and $s = s_{i-1}$ for $j = i - 1$. Note the symmetry $C_{i,j} = C_{j,i}$. The potential force does not depend on Re as it was obtained in the inviscid limit. This force acts symmetrically to both sides and tends to distribute the particles uniformly within the chain, and also splits the end bubbles off the chain because of missing neighbours.

It follows that the inviscid component of the bubble–bubble interaction force is a bi-directional short-range repulsive force that accelerates neighbouring bubbles symmetrically to both sides and does not depend on Re. The relative strength of the inviscid repulsion ($2C_{12}$) and the viscous attraction ($C_1 - C_2$) between two bubbles is shown in Fig. 4. The equality of these forces determines the value of the stable equilibrium distance. The pair is loosely coupled at high Re because of low ($C_1 - C_2$).

2.1.3. Bubble mass

Fluid exerts inertial resistance against the motion of an immersed body, the dynamic effect of which can be accounted for by an increase of the body mass by a certain amount (Lamb, 1932). For an isolated spherical particle in unbounded fluid this amount called 'added mass' equals one half of the body displaced fluid

$$m = 0.5 \times \frac{4}{3}\pi r^3 \rho. \tag{10}$$

Since a gas bubble in liquid is virtually massless, the added mass given by Eq. (10) represents its total mass. The single bubble added mass was also used for two bubbles in pairwise interactions by other authors (van Wijngaarden, 1993; Kumaran and Koch, 1993a, Kumaran and Koch, 1993b).

2.1.4. Equations of motion

The resulting acceleration reaction of a bubble is given by buoyancy, viscous, and inertial

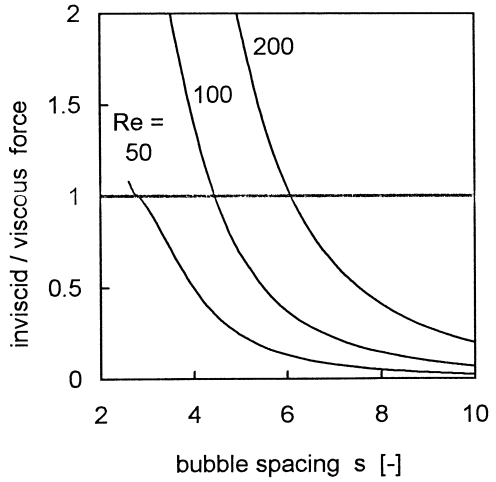

Fig. 4. Relative strength of the inviscid and viscous pairwise interaction forces: $2C_{12}/(C_1 - C_2)$.

forces. The buoyancy force is given by

$$B_i = \frac{4}{3}\pi r^3(\rho - \rho_{\text{gas}})g \approx \frac{4}{3}\pi r^3 \rho g. \tag{11}$$

The equation of motion for bubble i in the nearest-neighbour approximation reads:

$$(\text{mass}_i) \times (\text{acceleration}_i) = \text{buoyancy}_i - \text{drag}_i + \text{repulsion}_{i+1} - \text{repulsion}_{i-1}, \tag{12}$$

which in symbols becomes:

$$m\dot{v}_i = B_i - D_i + P_{i,\,i+1} - P_{i,\,i-1}. \tag{13}$$

After substitution of Eqs. (5), (8), (10) and (11) the dimensional form of the model is:

$$\dot{v}_i = a + b\Big(- v_i^2 C_i + v_{i+1}^2 C_{i,\,i+1} - v_{i-1}^2 C_{i,\,i-1}\Big)$$

$$\dot{d}_i = v_i - v_{i+1}, \tag{14}$$

with the initial condition for bubble distances and velocities:

$$d_i(0) = d_{i0}, \quad v_i(0) = v_{i0}, \quad i = 1, \ldots, N. \tag{14a}$$

Different 'boundary conditions' at the ends of the chain discriminate between the two different kinds of chain in Fig. 1(a) and (b):

$$\text{Free-end chain: } v_0 = v_{N+1} = C_{1,\,0} = C_{N,\,N+1} = 0, \tag{14b}$$

$$\text{Fixed-end chain: } v_0 = v_1, \quad v_{N+1} = v_N, \quad d_0 \text{ and } d_N \text{ are given, } C_{1,\,0}(d_0),\ C_{N,\,N+1}(d_N). \tag{14c}$$

In the fixed-end chain, the first bubble velocity v_1 is given by the distance d_0 from the virtual preceding bubble 0 and the last bubble experiences upward repulsive force from the virtual trailing bubble $N+1$. For brevity, it is put:

$$a = 2g, \quad b = 3/4r. \tag{15}$$

2.1.5. Validity range and model parameters

The model is supposed to be valid for Reynolds number 50–200 and bubble spacing $s > 2.6$. The bubble radius is fixed to $r = 0.4$ mm, which represents the characteristic length scale. An air 0.8 mm diameter bubble in water rises at about $v_0 = 15$ cm/s of velocity (Duineveld, 1995; Maxworthy et al., 1996), which represents the characteristic velocity scale. The characteristic time is given by r/v_0. Reynolds number remains the only free parameter of the model.

2.1.6. Numerical methods

The following numerical methods were used (Press et al., 1986). Nonlinear algebraic equations for steady states were solved by the Newton method. The equations of motion were integrated by the Adams–Bashford predictor–corrector method. These methods were used as

they are implemented in the professional software package Mathematica 3.0 (Wolfram, 1996). A more sophisticated analysis of the phase space (continuation of steady states on the parameter, stability and bifurcation analysis) was performed with the computer program CONT (Marek and Schreiber, 1995). The RRCHAOS program (Schouten and van den Bleek, 1996) was used for the analysis of chaotic signals (fractal dimension, Kolmogorov entropy). Guckenheimer and Holmes (1986) provides a survey of the dynamical systems theory and terminology.

2.2. Non-local interactions of bubbles (distant effects)

There are several reasons for adopting the nearest-neighbour approximation: (1) It is natural to start with the simplest case and assume that the dominant effects come from the nearest neighbours. (2) There are reliable data for drag force on a bubble pair by YP, whilst almost nothing is known about the effect of distant bubbles. (3) Numerous experimental and numerical data (see Section 1) support the assumption that the trailing drag does not depend on the position in the chain. (4) Even in the nearest-neighbour approximation, the model is able to reproduce the key phenomena observed in experiments (see Section 4). Non-local interactions substantially complicate the chain description because every bubble obeys a different drag law depending on its position. This breaks the chain symmetry. To make the analysis complete, it is necessary to quantify distant interactions and to explore their effects on chain behaviour. Expressions for distant interaction forces are given in this section.

2.2.1. Viscous distant effects

There are several ways to find the effect of distant preceding particles on the drag of a given particle:

1. The wake model suggested for two bubbles by KM can be adopted to more bubbles. The first step has recently been done by H97, and a divergent series was obtained of liquid velocity disturbances created by passing bubbles.
2. H97 suggested an approach how to calculate drag on farther bubbles down the chain. The method consists in successive calculation of the vorticity distribution around a bubble (diffusion equation) and in the wake between bubbles (vorticity equation). Although the idea is clear the calculations are not simple.
3. A detailed numerical study of the Navier–Stokes equation for three and more bubbles can be performed, following the approach of YP, but it would be difficult.

The first choice is sufficient for the purpose of this study. The KM model will be adopted and the divergence of the series avoided.

2.2.1.1. Estimates based on the KM model (limit drag C^*).

1. *Without viscous correction*. KM assumed that the trailing bubble of the pair trails in the wake of the leading bubble and experiences an additional velocity, hence, rises faster. This additional velocity was expressed by the average over the bubble cross-section area of the standard wake velocity profile

$$u_{w,\,1} = 0.5 C_0 v_0 \left(1 - \exp\left(-\frac{Re}{8 s_1}\right)\right), \tag{16}$$

where s_1 is the distance from the preceding bubble. H97 expressed the cumulative velocity disturbance generated by m preceding bubbles with spacing s_0 as linear superposition of the individual contributions

$$u_{w,\,m} = 0.5\, C_0 v_0 \sum_{j=1}^{m} \left(1 - \exp\left(-\frac{Re}{8 j s_0}\right)\right). \tag{17}$$

The summands go like $1/j$ for large j and the series diverges logarithmically for $m \to \infty$. However, for a finite number of preceding bubbles, the resulting drag coefficient can be calculated. Bubble n rises in fluid disturbed by $n-1$ preceding bubbles and its drag is given by use of Eq. (2) as:

$$C_n = 8gr/3(v_0 + u_{w,\,n-1})^2. \tag{18}$$

Fig. 5 shows the drag coefficients C_n (full lines) affected by the non-local interactions for several values of n. The drag decrease down the chain is substantial. Drag falls to zero for large n, which is not realistic but the results for low n are sensible. Namely, the value of C_2 (no distant effects) is close to the YP value.

2. *With viscous correction*. The divergence of the series (17) can be avoided by accounting for viscous dissipation in fluid. The standard wake profile used by KM results from timeless balance between convection and diffusion of the conserved fluid momentum (Batchelor, 1967). This eternal profile, not subjected to viscous decay, can be a useful approximation on time scales shorter than the viscous time scale L^2/ν. On longer scales, however, the velocity

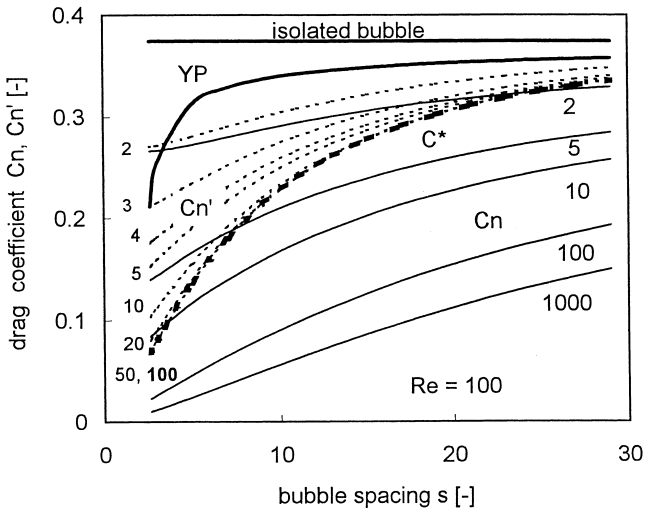

Fig. 5. Non-local bubble drag from the KM model. Drags $C_{2,\,5,\,10,\,100,\,1000}$ without viscous correction (full lines) fall to zero. Drags $C'_{2,\,3,\,4,\,5,\,10,\,20,\,50,\,100}$ with viscous correction (dotted lines) converge to the limit C^* (bold dotted line). YP drag (= nearest-neighbour approximation) and single bubble drag (bold full lines) ($Re = 100$).

disturbances created by bubbles die out as

$$\frac{u}{u_0} \sim \exp\left(- \frac{\nu t}{L^2} \right), \tag{19}$$

which weakens the distant effects. L is a characteristic length scale, r say, and the time t since the passage of bubble j is given by $js_0 r/v_0$. The viscous correction factor α can be defined

$$\alpha_j = \exp\left(- \frac{2js_0}{Re} \right), \tag{20}$$

by which the series (17) should be multiplied. The corrected series reads:

$$u'_{w,\,m} = 0.5 C_0 v_0 \sum_{j=1}^{m} \left(1 - \exp\left(- \frac{Re}{8js_0} \right) \right) \cdot \left(\exp\left(- \frac{2js_0}{Re} \right) \right). \tag{21}$$

The summands go like e^{-j}/j for large j and the series converges to a limit $u'_w(Re, s_0)$ for $m \to \infty$. The formula (18) for the corrected drag then becomes

$$C'_n = 8gr/3\left(v_0 + u'_{w,\,n-1}\right)^2 \tag{22}$$

and gives sensible results also for large n. Fig. 5 shows the drag coefficients C'_n (dotted lines) for several values of n. Corrected drag coefficients take more realistic values and converge to the limit curve $C^*(s_0, Re)$ (bold dotted). The convergence is rapid and the curves C_{50} and C_{100} coincide. The value of C_{100} is, therefore, taken as an acceptable approximation of the limit C^* in calculations. The existence of the limit results from balance between creation and decay of liquid velocity disturbances. This fact has a very important implication for the chain drag; after the passage of a certain number of bubbles, the drag coefficient takes the limit value C^*, which is the same for all following bubbles. For 0.8 mm diameter bubbles with a velocity of 15 cm/s and a spacing 20 bubble radii, it takes about 6 s for one hundred of them to pass and reach the equilibrium drag. This means that after a short time *all bubbles in the chain obey the same drag law C^* regardless of their position in the chain*. The distant effects are thus eliminated and the symmetry of the chain is recovered. The only result of distant effects is that the actual chain drag is lower than the nearest-neighbour YP drag (compare curves C^* and YP in Fig. 5). This is, in effect, equivalent to an increase of Re. The limit chain velocity is given by putting C^* into Eq. (2):

$$v^* = \left(\frac{8gr}{3C^*} \right)^{0.5}. \tag{23}$$

This approach based on the KM wake model is fruitful and gives some insight into the mechanism of the collective drag reduction. It seems, however, that this model, based on the steady far-wake velocity profile behind each bubble, tends to overestimate the distant effects. At low spacing, the predicted distant drag is roughly four times lower than the local drag and roughly by one order smaller than the single bubble drag, Fig. 5. The velocity

disturbances introduced by bubbles are hardly developed into the steady far-wake profile. Moreover, the profile does not remain intact, but is run over and destroyed by all following bubbles. This weakens the distant effects further more. Therefore, the limit drag C^* represents the *lower bound* of the real chain drag. On the other hand, the nearest-neighbour YP drag (4) represents the *upper bound* of the real chain drag. Formulas like (21) should be weighted by a coupling factor, which expresses the strength of the non-local interactions. The approach suggested below is compatible with the present model and includes such a coupling parameter.

2.2.1.2. Estimates based on the YP model (limit drag C^{**}). The distant effects can also be introduced into the model (14) in the following way. We assume that the final effect of all preceding bubbles is proportional to the sum of YP corrections (4) to the single bubble drag factor $F = 2.2$. Because these effects decay with time due to viscosity, the sum must be multiplied by the viscous correction factor α given by Eq. (20). The following drag factors are obtained for bubbles 2, 3, and n:

$$F_2 = 2.2 + f_{2,\,1}$$

$$F_3 = 2.2 + f_{3,\,2} + k\alpha_{(3-1)} f_{3,\,1}$$

$$F_n = 2.2 + f_{n,\,n-1} + k\sum_{j=1}^{n-2} \alpha_{n-j} f_{n,\,j}, \quad 0 \le k \le k_m, \text{ (Non-local interactions)} \tag{24}$$

where $f_{n,\,j}$ is the effect of bubble j on the drag of bubble n behind it and $s_{n,\,j}$ is their distance,

$$f_{n,\,j} = 2.5\left(s_{n,\,j} - 2\right)^{-0.6}, \quad s_{n,\,j} = \sum_{k=j}^{n-1} s_k, \quad j = n-1, n-2, \ldots, 2, 1. \tag{25}$$

The distance $s_{n,\,j}$ equals $(n - j - 1)s_0$ for a chain with uniform spacing s_0. The summands in Eq. (24) go like $e^{-j}/j^{0.6}$ for large j and the series converges to a limit $f(Re, s_0, k)$ for $n \to \infty$. Drag coefficients C_n calculated by putting Eq. (24) into Eq. (6) converge to the limit curve $C^{**}(s_0, k, Re)$, of which C_{100} gives a sufficient estimate. The convergence is rapid, and C_3 differs from the limit by 10%, and C_{20} by 3% (calculated for $Re = 100$ and $k = 0.1$). Again, this means that after the passage of several dozens of bubbles, all following bubbles obey the same drag law. The proportionality constant k stands for the *strength of the non-local coupling among bubbles*. The value of k can be changed continuously in the model to explore the effect of distant interactions in a wide range. The value of k varies from zero to a maximum value k_m. For zero coupling, C^{**} coincides with its upper bound, the YP drag. For the maximum coupling, C^{**} reaches its lower bound C^*; this happens at the smallest permitted spacing $s = 2.6$ and gives $k_m \cong 0.44$. Fig. 6 shows the limit drag C^{**} (dotted lines) for several values of k. The bold dotted line represents the limit drag at the maximum coupling, the lowest distant

drag considered here. Similarly as in Eq. (23), the chain velocity v^{**} is obtained by putting C^{**} into Eq. (2).

It follows that the non-local viscous interactions can not generally be neglected. This is due to the long-range nature of these forces and their asymmetric, unidirectional, and cumulative character. These effects are considered in this study and incorporated into the model merely by replacing the local formula (4) with the distant formula (24).

2.2.2. Inviscid distant effects

Inertial effects due to body motion in fluid manifest themselves in two ways: (1) by effective increase of body mass and (2) by pressure forces on other bodies. In the nearest-neighbour approximation, the isolated particle added mass was used for all bubbles in the chain and the inviscid two-body force formula was used for multi-body system. The error being made is estimated here.

2.2.2.1. Added mass. The added mass is basically a tensor quantity (Batchelor, 1967) whose elements are the inertial coefficients. Values of these coefficients depend on positions and shapes of all surfaces presented in the fluid. These coefficients are also called added mass coefficients, and represent the portion of the body-displaced fluid to which the added mass equals:

$$c = \frac{(\text{added mass})}{(\text{body volume})\rho_{\text{fluid}}}. \tag{26}$$

For a *single* particle, the added mass coefficient is $c_0 = 1/2$. For *two* equal particles moving in

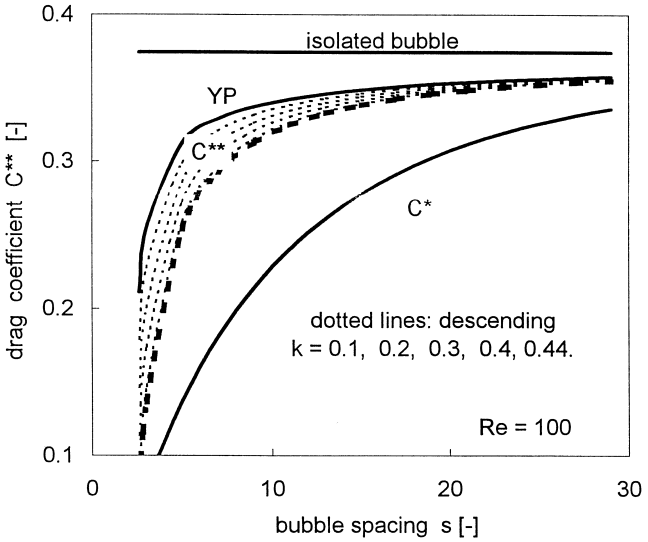

Fig. 6. Non-local bubble drag from the YP model. Limit drag C^{**} (dotted lines) falls with increasing distant coupling k. Minimum limit drag corresponds to maximum coupling $k_m = 0.44$ (bold dotted line). The family of C^{**} curves is limited (bold full lines) from above by the YP drag (upper bound) and from below by the KM limit drag C^* (lower bound) ($Re = 100$).

line of centres, there are three inertial coefficients (Lamb, 1932, Article 98):

$$L = N = c_0\left(1 + 3(s^2 - 1)^{-3} + \cdots\right) \sim s^0 + s^{-6} + \cdots$$

$$M = 3c_0 s^{-3}\left(1 + (s^2 - 2)^{-3} + \cdots\right) \sim s^{-3} + s^{-9} + \cdots. \tag{27}$$

Thus, the addition of one more particle causes effects only of $O(s^{-3})$ to the single particle value $O(s^0)$. Such effects are weak and will be neglected in this study. For *more* particles in line with uniform spacing, two important results were obtained (Michael, 1965; Helfinstine and Dalton, 1974). First, at larger spacing, all particles have the same and constant value of the added mass equal to c_0. For example, in a long chain, about 90% of the single particle value is reached at $s = 4$. Second, at low spacing (in a chain with five and more particles), the added mass of all interior particles is the same (i.e. depends on distance in the same way) and is slightly lower than c_0. This means that all inner particles experience the same acceleration reaction to the applied force. The symmetry of the chain is not broken. Only the two end particles of a finite chain have a slightly higher mass than the rest.

It follows that the use of a constant value of added mass for more bubbles in chain is an acceptable approximation. In this study, where very low spacing or touching of bubbles is excluded and bubble separation is typically not extremely low, the single bubble value c_0 is applied.

2.2.2.2. Inviscid force. The inertial coefficients like L, M, and N are also coefficients of the quadratic form of the kinetic energy of the fluid-particle system. The potential interaction force is given by the derivatives of these coefficients with respect to co-ordinates (Lamb, 1932, Article 135–136).

For the interaction of *two* particles, the leading order force term $O(s^{-4})$ comes from the spatial derivative of the coefficient M with error $O(s^{-7})$. This force is given by Eqs. (8) and (9) and is used in the nearest-neighbour approximation. In this approximation, with single particle added mass applied to both particles, the Lagrange equations of motion for two particles given by Lamb (1932, Article 138 and used by YP Eq. (5.1)) reduce to the local-interaction model suggested in this study (Eq. (14)). The fact that this model agrees well with YP results provides support for neglecting the distant inertial effects. For interaction of *more* particles, the inertial coefficients of all inner particles display the same dependence on distance (Michael, 1965; Helfinstine and Dalton, 1974) so that their spatial derivatives are also the same. Thus, the *particles obey the same force law regardless of their position* in the chain. The inviscid force is expected to equal the two-body force (Eq. (8)) at larger spacing and to be slightly modified at lower spacing.

If the distant effects are approximated by linear superposition of the two-body force (Eq. (8)), the total inertial force on bubble n in Eq. (13) becomes

$$P_{\text{pot},\,n} = \frac{1}{2}\rho\pi r^2\left[\sum_{j>n} v_j^2 C_{n,\,j} - \sum_{j<n} v_j^2 C_{n,\,j}\right], \quad C_{n,\,j} = 12 s_{n,\,j}^{-4}, \tag{28}$$

and depends on positions and velocities of all neighbours. Assuming that the particle velocities

in the chain are comparable, which is reasonable, the total inertial force coefficient of bubble n is given by the symmetric composition of the identical contributions from neighbours on both sides,

$$C_{\mathrm{pot},\,n} \sim \sum_{j>n} C_{n,\,j} - \sum_{j<n} C_{n,\,j}. \tag{29}$$

The effect of the kth neighbour falls as $(ks_0)^{-4}$, so that the relative strength of neighbours 1, 2, 3, 4, ... is 1, 1/16, 1/81, 1/256, ... and the inviscid interactions are controlled mainly by the nearest neighbours. This rapid fall with distance also makes the effects of unequal number of left and right neighbours negligible. The distant inertial effects, therefore, do not break the symmetry of the chain. The inertial coefficients of the two outer bubbles differ slightly from the rest. These bubbles do not occur in the fixed-end chain. In the free-end chain, the dominant asymmetry of the first bubble is given by the different drag law and that of the last bubble by the missing neighbour. These 'first-order effects' are much stronger than the asymmetry caused by the different value of the inertial coefficients at a spacing typically occurring in this study. The distant inertial coupling might become important in a purely inviscid chain. These subtle effects would possibly affect the structure of the Hamiltonian dynamics, which is oversensitive and inherently unstable on its own.

It follows that the non-local inviscid interactions can be neglected. At bubble spacings relevant to this study, the inertial coupling is weak both absolutely and relatively, compared with the viscous coupling (compare summands in Eqs. (24) and (29)). This is due to the rapid fall of the inertial forces with distance and their symmetric character. The nearest-neighbour approximation of the potential interactions will be used throughout in this study.

3. Results

3.1. Free-end bubble chain

The relevant equations of motion are (14) with the free-end boundary condition (14b). Notions 'low Re' and 'high Re' refer to the model range $Re = 50$–200.

3.1.1. Two bubbles

The model validation is given here by comparison with the YP results, which are supposed to be correct. YP predicted a steadily rising pair separated by an equilibrium distance. Equations of motion for the leading bubble 1 and trailing bubble 2 become:

$$\dot{v}_1 = a + b\left(-v_1^2 C_1 + v_2^2 C_{1,\,2} - 0\right)$$

$$\dot{v}_2 = a + b\left(-v_2^2 C_2 + 0 - v_1^2 C_{2,\,1}\right)$$

$$\dot{d}_1 = v_1 - v_2. \tag{30}$$

Steady state. A steady state (equilibrium point, stationary solution) represents the long-time behaviour of the chain, which is reached from a given initial condition after a temporal transition period. A stable steady state of an N-bubble chain means that all N bubbles with equal velocities rise together in one piece. An unstable steady state or the absence of the stationary solution mean that this is not possible and that the chain must split into smaller fragments. The steady values of distances and velocities depend on the model parameters, here on Re only.

The steady state condition for the pair is: $v_1 = v_2$ and $C_1 - C_2 = 2C_{1,2}$. The latter relation means: attraction = repulsion, see Fig. 4. Obviously $C_1 > C_2$ and the difference $C_1 - C_2$ holds the pair together. Fig. 7 shows the parameter dependence of the steady pair spacing, which compares well with YP. The slight departure from YP data is the price for avoiding the dependence on Re of factors $F_{1,2}$ in the present model. The equilibrium drag coefficients are ordered $C_0 > C_1 > C_s > C_2$ and shown in Fig. 8. The steady pair drag C_s is the mean drag of the pair. The pair is always faster than a singlet because the pair is more streamlined. This is especially true at low Re, where the trailing drag reduction is high, the attractive force is large, and the pair is strongly compressed. The pair drag reduction is mainly due to low C_2 since C_1 practically equals the single bubble drag. The trailing drag increases faster with spacing than it falls with Re at low Re, which causes the hump in the C_2 graph. The steady pair velocity is given by:

$$v_s = \left(\frac{a}{bC_s}\right)^{0.5} = \left(\frac{8gr}{3C_s}\right)^{0.5}, \quad C_s = \frac{(C_1 + \cdots + C_n)}{n}. \tag{31}$$

The pair velocity follows the single bubble formula (2) and (31) holds for any steady bubble fragment with n bubbles.

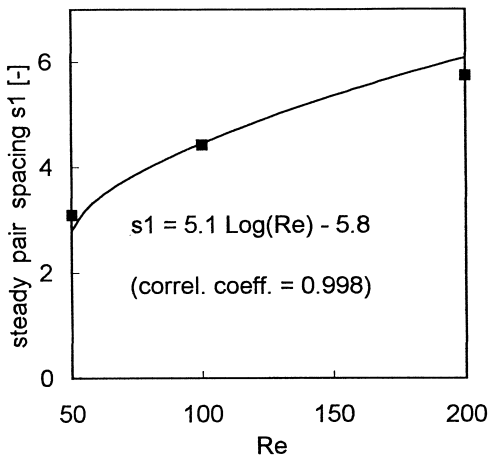

Fig. 7. Free-end chain. $N = 2$. Parameter dependence of steady pair spacing: Model (line), YP data (marks) ■.

Transient dynamics. The equilibrium point is a stable node with real negative eigenvalues of order -10^1 and -10^2 giving the characteristic time scales associated with relaxation of small perturbations of 0.1–0.01 s. The orientation of the eigenvectors in the phase space at the equilibrium point makes the velocities fast variables and the distance slow variable with their characteristic time scales separated by a gap of more than one order. The fast mode behaviour can be neglected in the long-time horizon, where the dynamics is governed by the slow modes and it is sufficient to pay attention to the distances only. The pair transition dynamics is rather simple; reaching the stable equilibrium from all possible initial conditions. The solutions shown in Fig. 9 correspond to Fig. 12–14 in YP. The present model compares well with the YP data. The discrepancy at early times is ascribed to the development of the boundary layer on the bubbles (10–20 units of the nondimensional time), which is not covered by the present model.

It follows that the model reproduces the basic features of the pair dynamics well. This justifies the use of the single particle added mass and the leading order term expression for the inviscid force.

3.1.2. Three bubbles

3.1.2.1. Local interactions. The relevant equations of motion are (14) with the local drag (7). There are two trailing bubbles 2 and 3 following the same drag law $F_2 = F_3$.

Steady states. Again, the steady state condition expresses the force balance between attraction and repulsion for the three bubbles. Unlike the case of two bubbles, there is no steady solution for $Re < 135$ so that the long-time chain is broken into fragments and the only attractor is infinity being approached along d_2 direction. This corresponds to fast leading pair 1&2 followed

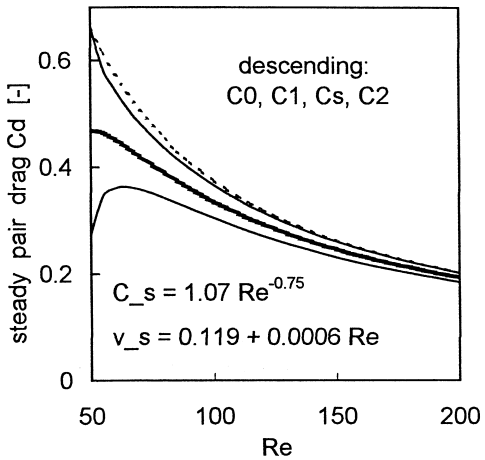

Fig. 8. Free-end chain. $N = 2$. Parameter dependence of steady pair drag coefficients: $C_0 > C_1 > C_s > C_2$. Correlations for steady pair drag C_s and velocity v_s.

by slow singlet 3 with distance d_2 between them diverging in time. Two steady solutions are created by saddle-node bifurcation at the limit point $Re \approx 135$. The stable node represents the stable equilibrium triplet 1&2&3 and the (unstable) saddle corresponds to two fragments, the leading doublet and trailing singlet. The initial conditions yielding triplets lie in the basin of attraction of the node, Fig. 10. Above the separatrix line, triplets cannot be formed. Fig. 11 shows the parameter dependence of the stationary branches. The steady spacing s_1 in the triplet is always smaller than s_2 (and also slightly smaller than that in the doublet), because the second bubble is pushed upwards by the third bubble. Bubble 3 is repelled farther from the pair due to the missing neighbour behind it. The steady drags are ordered $C_0 > C_1 > C_s > C_3 > C_2$ and shown in Fig. 12. The individual drags in a triplet are slightly less than those in a pair, so that the triplet is slightly faster.

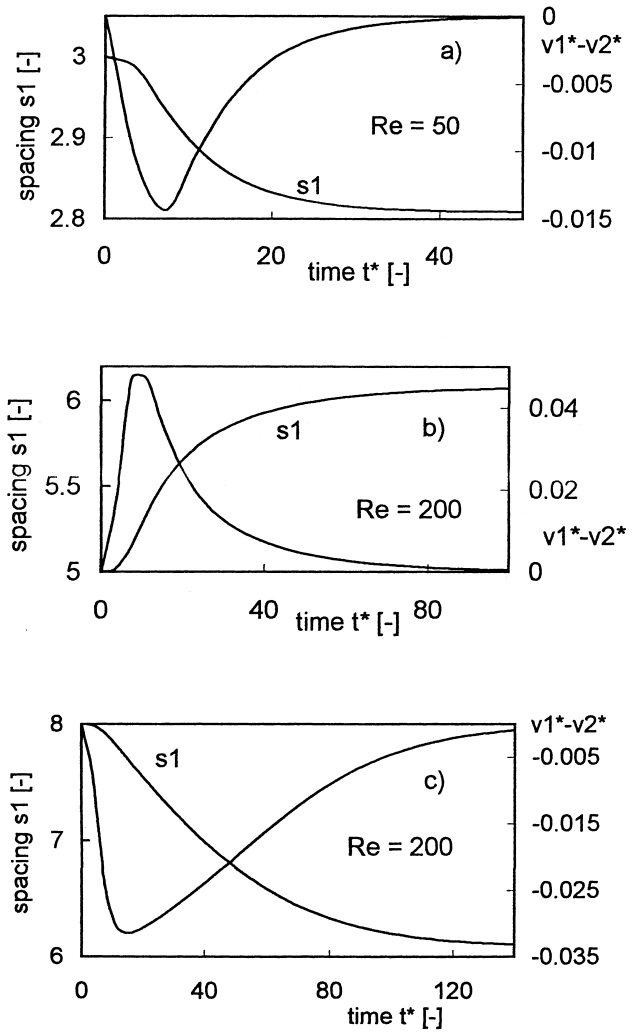

Fig. 9. Free-end chain. $N = 2$. Transition dynamics of pair. Initial spacing $s = 3$ (a), $s = 5$ (b), and $s = 8$ (c). Initial velocities $v_{1,2} = 0$. (Time scaled by r/v_0, velocities by v_0).

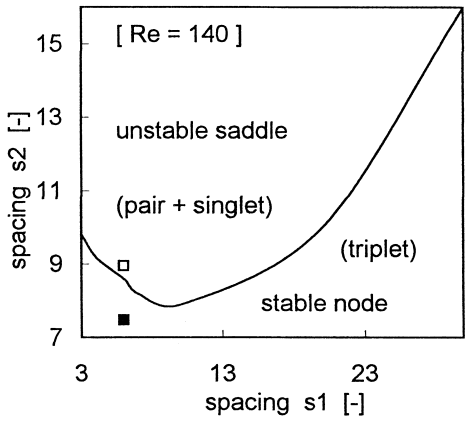

Fig. 10. Free-end chain. $N = 3$. Phase plane (s_1, s_2): initial conditions for triplet lie below the separatrix line, conditions for fragmented chain (doublet and singlet) above the line ($Re = 140$).

Dynamic behaviour.

1. *Triplet formation*: The physical reason for the saddle-node bifurcation yielding the triplet is the following. Bubble 2 catches the slow bubble 1 and forms fast leading pair 1&2 that escapes. To join this pair, bubble 3 must come close and reduce its drag to the pair level. If the drag difference between the doublet and singlet is large, especially at low *Re*, Fig. 8, the singlet must come very close, which is impossible due to the strong repulsion. The drag difference falls with increasing *Re* making the merger possible for $Re > 135$.
2. *Re-pairing*: If a leading singlet is attacked by a trailing pair from below and a triplet cannot be formed, re-pairing occurs. Bubble 1 attracts bubble 2 by wake suction, drag C_2 is reduced as well as the difference $C_2 - C_3$ holding the pair 2&3 together. The pair expands and slows down. Bubble 2 is attracted by bubble 1 and repelled from bubble 3. When spacing d_2 reaches the value corresponding to the equilibrium leading pair spacing, the trailing pair

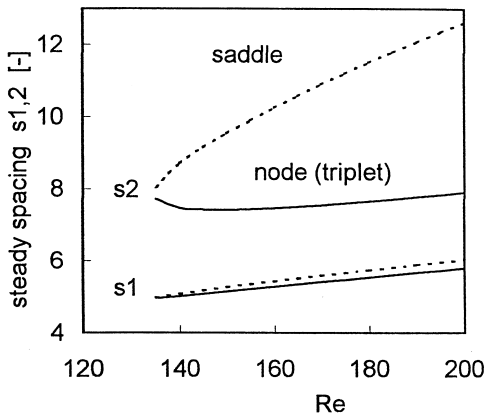

Fig. 11. Free-end chain. $N = 3$. Parameter dependence of steady solution: stable node = triplet (full lines), unstable saddle = two fragments, doublet and singlet, (dotted lines).

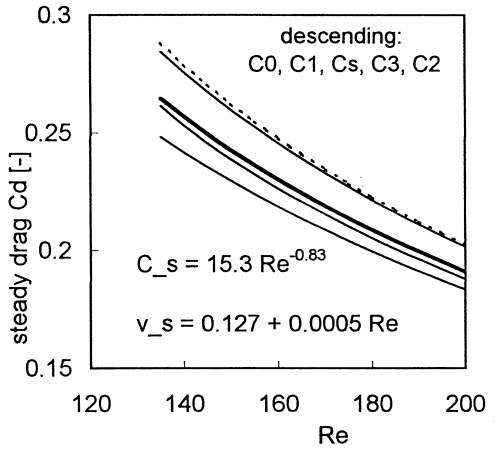

Fig. 12. Free-end chain. $N = 3$. Parameter dependence of steady triplet drag coefficients: $C_0 > C_1 > C_s > C_3 > C_2$. Correlations for steady triplet drag C_s and velocity v_s.

2&3 splits and the leading pair 1&2 forms and accelerates, leaving bubble 3 behind. Re-pairing is thus completed, see Fig. 13 (full lines).

3. *Collision dynamics*: Re-pairing is essentially a dynamic phenomenon consisting in the exchange of a bubble between two fragments. This is a typical phenomenon in chain collision dynamics. In the nearest-neighbour approximation, three bubbles are enough to simulate an early stage of a two-fragment collision. A test pair stands for the fragment under study and a singlet placed either ahead or behind the test pair simulates the effect of the approaching fragment. A bubble placed ahead *destabilises* the pair; the pair expands, slows down, and loses its pivot. The pivot is easily split at high *Re*, where the bubble ahead

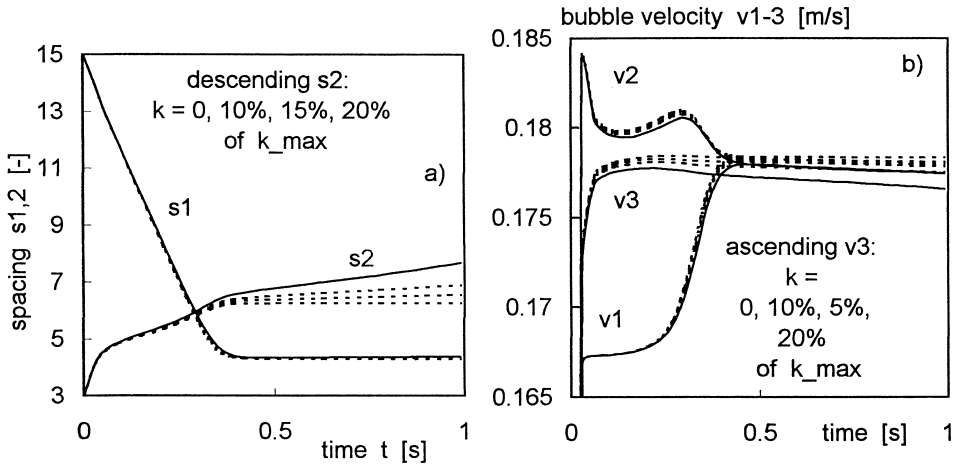

Fig. 13. Free-end chain. $N = 3$. Re-pairing. Bubble distances (a) and velocities (b) versus time. Nearest-neighbour approximation (full lines). Distant effects (dotted lines): descending $k = 0.044$, 0.066, and 0.088. Initial spacing $s_1 = 20$, $s_2 = 5$ and velocities $v_1 = v_2 = 0$ ($Re = 100$).

is 'felt' from a large distance, Fig. 14 (full lines). A bubble placed behind *stabilises* the pair; the pair is compressed from below, made streamlined and faster, Fig. 14 (dotted lines).

3.1.2.2. Non-local interactions. The relevant equations of motion are (14) with the non-local drag (24). Compared with bubble 2, the drag of bubble 3 is additionally reduced by the velocity disturbances created by the distant bubble 1: $F_2 < F_3$ and $C_2 > C_3$. Bubble 3 has *lower drag* than bubble 2 (when equally spaced, of course).

Steady states. Calculations show that the critical point in Fig. 11, where the steady solution appears, shifts to the left while increasing the coupling parameter k. The following values were found: $Re_c = 135, 130, 125, 120, 94, 57$, for $k = 0, 0.01, 0.02, 0.03, 0.1, 0.3$. The Reynolds number range for triplet formation $Re > Re_c$ expands and the re-pairing range $Re < Re_c$ reduces. The true value of k can be determined experimentally by finding the critical value of Re, where three closely spaced bubbles merge into the triplet. Due to the distant coupling between bubbles 1 and 3, the total triplet drag is reduced and the velocity increased.

Dynamic behaviour.

1. *Triplet formation*: The drag difference between the fast leading pair 1&2 and the singlet 3 is reduced by the distant coupling (low C_3) so that the triplet can form at lower Re.
2. *Re-pairing*: The process of re-pairing is not affected much when the coupling is weak. However, at about 20% of the maximum coupling, the merger of the two fragments occurs instead of re-pairing. The drag C_3 is so low that the trailing pair survives the collision and does not split; spacing s_2 settles at a constant value, Fig. 13 (dotted lines).

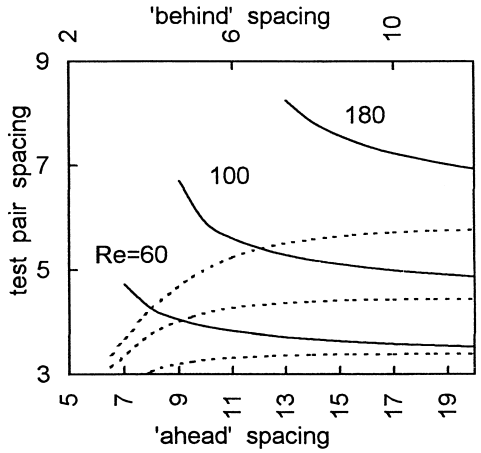

Fig. 14. Free-end chain. $N = 3$. Collision dynamics. A bubble ahead of the test pair causes expansion and breakup of the pair (end points of the full lines). A bubble behind causes compression of the pair (dotted lines). Ascending: $Re = 60, 100, 180$.

3.1.3. Four bubbles

3.1.3.1. Local interactions.

Steady states and periodic orbits. The typical feature of a four-bubble chain is the interaction of two pairs: merger, separation, oscillation, pairing-off, and re-pairing. No steady solution was found for $Re < 51$, where the chain splits into two fragments, two pairs, with the diverging distance between them. Two stationary solutions were found for Re 51–87, the stable and unstable branch. The stable branch representing the equilibrium quadruplet 1&2&3&4 is a stable node for Re 51–65 and becomes a stable centre for Re 66–87. The centre loses stability and undergoes Hopf bifurcation at $Re \approx 87$, where a stable periodic solution — the limit cycle — branches off. The limit cycle loses stability at about $Re \approx 110$ and infinity remains the only attractor. It is first approached along d_2 direction, where the chain spontaneously splits into pairs: pairing-off. The orientation of the eigenvectors changes at $Re \approx 135$ and the diverging direction becomes d_3. One bubble is exchanged between the two pairs, and they recombine into the leading triplet 1&2&3 and trailing singlet 4 via re-pairing. The initial conditions determine which attractor will be approached, see Table 1. Fig. 15 shows the parameter dependence of the stable branch corresponding to the steady spacing in the quadruplet. The quadruplet drag coefficients are ordered $C_0 > C_1 > C_3 > C_s > C_4 > C_2$ and shown in Fig. 16.

Dynamic behaviour.

1. *Pairing-off*: Pairing-off is the archetype of free-end chain behaviour. Pairing-off is usually the first step in the chain evolution from a uniform initial spacing. The dynamics of pairing-off is simple: bubble 2 approaches bubble 1, fast pair 1&2 forms, accelerates, and escapes. Bubble 3 acquires the large single bubble drag and becomes the new pivot of the rest of the

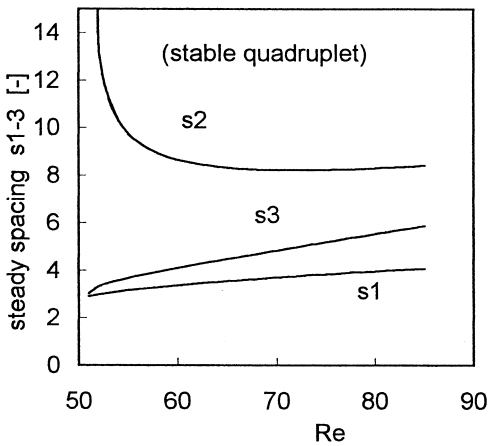

Fig. 15. Free-end chain. $N = 4$. Parameter dependence of steady bubble spacing in quadruplet (in nearest-neighbour approximation the solution exists for Re 51–87).

Table 1
Free-end chain. Long-time quasi-steady fragmented chain structure for several values of Reynolds number and initial spacing[a]

N	s_0	Re							
		60	80	100	120	140	160	180	200
3	3	2+1	2+1	2+1	2+1	3	3	3	3
	10	2+1	2+1	2+1	2+1	2+1	2+1	3	3
	50	2+1	2+1	2+1	2+1	2+1	2+1	2+1	2+1
4	3	4	2+2	2+2	2+2	3+1	3+1	3+1	3+1
	10	4	4	4*	2+2	3+1	3+1	3+1	3+1
	50	2+2	2+2	2+2	2+2	3+1	3+1	3+1	3+1
5	3	4+1	4+1	4*+1	2+2+1	3+2	3+2	3+2	3+2
	10	4+1	4+1	4*+1	2+2+1	3+2	3+2	3+2	3+2
	50	2+2+1	2+2+1	2+2+1	2+2+1	3+2	3+2	3+2	3+2
6	3	4+2	4+2	4*+2	2+2+2	3+2+1	3+2+1	3+2+1	3+2+1
	10	4+2	4+2	4*+2	2+2+2	3+2+1	3+2+1	3+2+1	3+2+1
	50	2+4	2+4*	2+2+1+1	2+2+2	[3+3]	[3+3]	[3+3]	[3+3]
7	3	4+2+1	4+2+1	4*+ 2+1	2+2+2+1	[3+3]+1	[3+3]+1	[3+3]+1	[3+3]+1
	10	4+2+1	4+2+1	4*+2+1	2+2+2+1	[3+3]+1	[3+3]+1	[3+3]+1	[3+3]+1
	50	2+4+1	2+4*+1	2+2+1+1+1	2+2+2+1	[3+3]+1	[3+3]+1	[3+3]+1	[3+3]+1
8	3	6+2	6+2	4*+2+2	5+2+1	[3+3]+2	[3+3]+2	[3+3]+2	[3+3]+2
	10	4+4	4+4*	4*+2+2	5+2+1	[3+3]+2	[3+3]+2	[3+3]+2	[3+3]+2
	50	2+4+2	2+[4+2]*	2+2+1+1+1+1	2+(5)+1	[3+3]+2	[3+3]+2	[3+3]+2	[3+3]+2
9	3	6+2+1	6+2+1	4*+2+2+1	5+3+1	[3+3+3]	[3+3+3]	[3+3+3]	[3+3+3]
	10	4+4+1	8+1	4*+2+2+1	5+3+1	[3+3+3]	[3+3+3]	[3+3+3]	[3+3+3]
	50	2+4+2+1	2+4*+2+1	2+2+1+1+1+1+1	2+(5)+2	[3+3]+2+1	[3+3]+2+1	[3+3]+2+1	[3+3]+2+1
10	3	6+4	6+2+2	4*+2+2+2	5+3+1+1	[3+3+3]+1	[3+3+3]+1	[3+3+3]+1	[3+3+3]+1
	10	4+4+2	8+2	4*+2+2+2	5+3+2	[3+3+3]+1	[3+3+3]+1	[3+3]+3+1	[3+3]+3+1
	50	8+2	2+[4+4]	2+2+1+1+1+1+1+1	2+2+(6)	[3+3+3]+1	[3+3+3]+1	[3+3]+3+1	[3+3]+3+1

[a] N: chain length, Re: Reynolds number, s_0: initial uniform spacing. Bubble groups: 2+4+1 — leading pair followed by quadruplet followed by singlet; 4* — oscillating quadruplet; [3+3] — two triplets too widely separated to be considered as hexaplet; (5) — five bubbles not settled down with distances varying on very long time scales. The fragments are ordered according to their rising velocities. Distances between fragments grow (almost linearly) with time. Initial velocities $v_i = 0$..

chain: bubble 3 is approached by bubble 4, fast pair 3&4 forms, accelerates, and escapes, etc. This viscous instability progresses farther downchain. The slowest bubble 1 in the free-end chain holds the rest like a compressed spring; once this keystone is removed, the rest explodes and splits into pieces. Drag C_1 roughly equals C_0 and is basically constant (no preceding wake). The only way to get rid of bubble 1 is to incorporate it into a fast group, the doublet here. Pairing-off does not occur at high *Re*, where the attraction in pairs is weak and the repulsion is strong. Pairing-off in a seven-bubble chain predicted by the model is shown in Fig. 18. The pairs thus formed undergo subsequent interactions resulting in the long-time chain structure that depend on *Re*, as reflected by the bifurcation sequence. The physical picture of the bifurcation sequence is the following.

2. *Quadruplet formation*: Quadruplet basically is a weak composition of two pairs. The drag difference between two similar fragments, two pairs, is low and they easily can merge at low *Re* (in contrast to two different fragments, doublet and singlet, in three-bubble chain). This actually happens at $Re = 51$.
3. *Oscillation*: A further increase of *Re* corresponds to increase of inertial effects. These effects are negligible in the overdamped dynamics of the stable node. However, at higher *Re*, the particles overshoot the equilibrium point in damped oscillations around the stable centre. As the inertial interactions increase further, the pairs start to disturb each other more and more, which results in persistent oscillations around the unstable centre. The mechanism of these oscillations is the following. The slightly faster trailing pair approaches the leading one from below. Coming closer, the trailing pair expands and slows down (effect of a bubble ahead) while the leading pair compresses and accelerates (effect of a bubble behind). The distance between the pairs increases again, both pairs relax back to normal, and we are where we started from. This 'breathing' of the pairs sustains stable nonlinear oscillations, see Fig. 17, which are made possible by the fragile balance between the inertial and viscous forces.

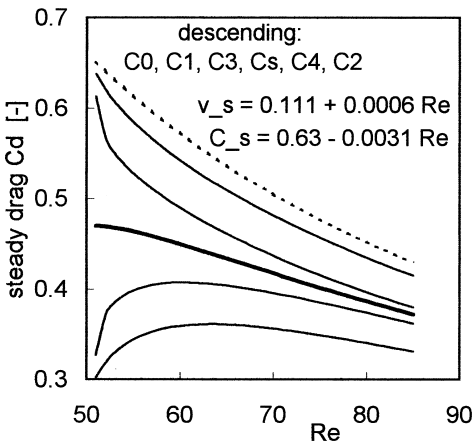

Fig. 16. Free-end chain. $N = 4$. Parameter dependence of steady quadruplet drag coefficients: $C_0 > C_1 > C_3 > C_s > C_4 > C_2$. Correlations for steady quadruplet drag C_s and velocity v_s.

4. *Fragmentation*: This subtle balance breaks at a higher *Re* and the pairs separate. At an even higher *Re*, the trailing pair comes close to the leading pair and is split by re-pairing.

3.1.3.2. Non-local interactions.

Steady states. The distant effects display the ambiguous Shiva tendency to both *create* and *destroy* stable equilibria. They change the nearest-neighbour solution in Fig. 15 in the following way. Both bifurcation points limiting the quadruplet range move to the left with increasing k: $Re \in [51, 87]$, [50, 82], [50, 79], [50, 75], [50, 58], [50, 50] for $k = 0$, 0.01, 0.02, 0.03, 0.1, 0.3.

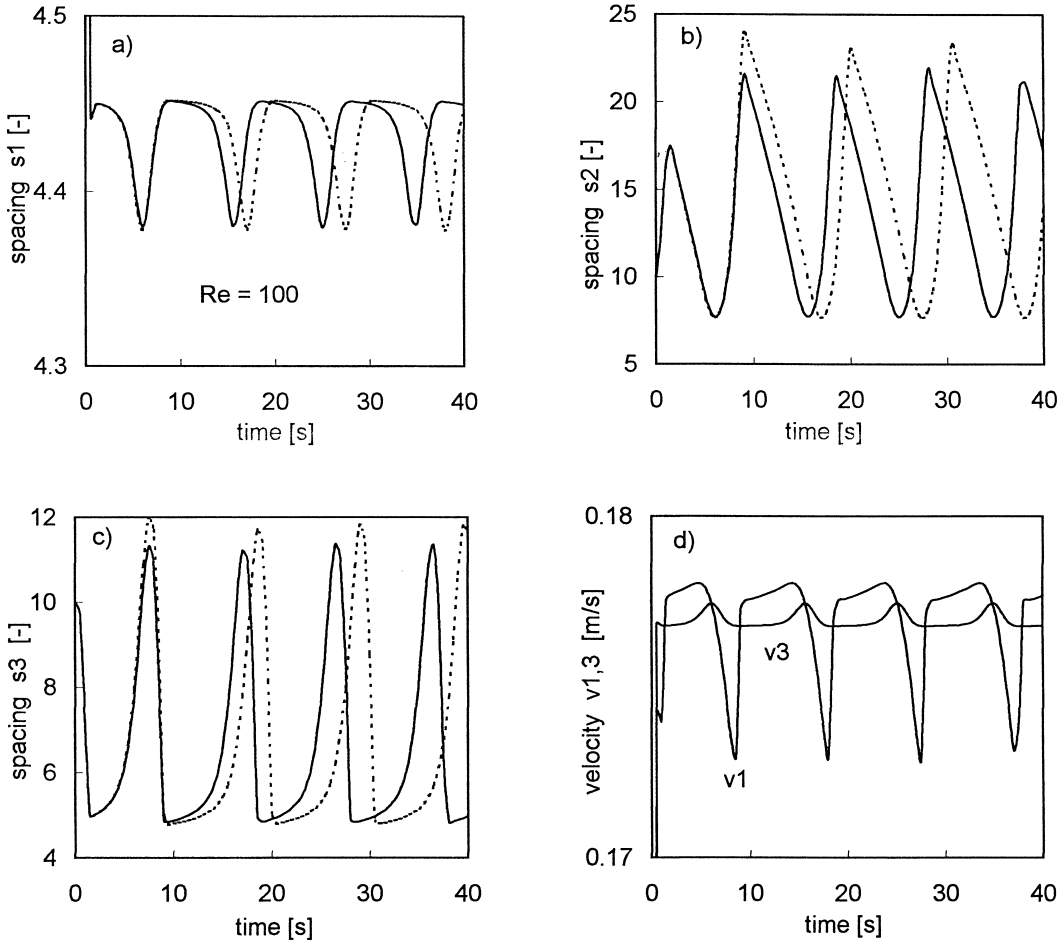

Fig. 17. Free-end chain. $N = 4$. Oscillations of rising quadruplet: bubble distances (a–c) and velocities (d). Nearest-neighbour approximation (full lines). Distant effects at $k = 0.001$ (dotted lines). Initial spacing $s_i = 10$ and velocities $v_i = 0$ ($Re = 100$).

The left point of the interval shifts to smaller values of *Re* for reasons already explained for the three-bubble chain. The right point moves the same way because the strong bounce of the pairs caused by distant effects make them oscillate sooner. Again, the value of k can be determined by finding the critical value of *Re* experimentally.

Dynamic behaviour. At *low Re*, the closely spaced quadruplet is destabilised and eventually split when increasing k. This is caused mainly by the inertial forces. The trailing pair has a considerably lower drag than the leading pair. The large deceleration on approach turns into a large collision force that makes the pairs oscillate. A further increase of k destroys the oscillation balance and the quadruplet splits into pairs. An even further increase of k shows the creative face. Bubbles 1, 2, and 3 are condensed into a triplet and then bubble 4 is added. The chain structure follows the sequence: $4 \rightarrow 4^* \rightarrow 2+2 \rightarrow 3+1 \rightarrow 4$ (see the legend of Table 1) with the transitions at $k = 0.08$, 0.24, 0.27, 0.55 (calculated for $Re = 60$ and initial values $s_0 = 3$, $v_0 = 0$). Highly separated bubbles are first brought together, made to oscillate, then separated again, to be eventually merged: $2+2 \rightarrow 4^* \rightarrow 2+2 \rightarrow 3+1 \rightarrow 4$ at $k = 0.18$, 0.24, 0.27, 0.55 ($Re = 60$, $s_0 = 50$). Weak coupling increases both the amplitude and period of the oscillations; both the spacing and the relaxation time are higher after a stronger bounce, Fig. 17. Similar tendencies were found at *medium Re*. The fusion of bubble fragments $2+2 \rightarrow 3+1 \rightarrow 4$ takes place at $k = 0.03$ and 0.26 ($Re = 120$, $s_0 = 3$). Distant effects break the oscillating quadruplet, split it into pairs, and then condense again, $4^* \rightarrow 2+2 \rightarrow 3+1 \rightarrow 4$ at $k = 0.019$, 0.09, 0.5 ($Re = 100$, $s_0 = 10$). *At high Re*, a new stable steady branch (and several unstable branches) is created at $Re = 200$ and progresses to lower *Re* reaching values 187, 155, 99, ... at $k = 0.17$, 0.2, 0.3, ... A quadruplet can thus be formed instead of triplet and singlet even at high *Re* due to non-local effects (cf. Table 1).

3.1.4. More bubbles

3.1.4.1. Local interactions.

Long-time chain structure. Long-time highly fragmented structures of chains up to 10 bubbles are presented in Table 1. The uniform initial spacing was chosen in simulations because it (1) lies on the diagonal of the phase space and passes through its central part and (2) is easy to produce experimentally. The resulting chains are composed of several quasi-steady bubble fragments of different lengths and velocities with diverging distance between them. The resulting chain structure displays certain recurrent features that are expected to repeat for longer chains. Due to the asymptotic nature of the interaction forces, bubbles may take a considerable time (10^2–10^5 s) to produce these quasi-steady patterns. Fragments affect each other from extremely long distances and their relative velocities are very low. This results in long-time unsteadiness of the chain dynamics.

Chain dynamics. The important elements of chain dynamics have already been discussed in the preceding sections. At low *Re*, pairing-off typically starts the evolution of a chain with a uniform spacing, Fig. 18. The released pairs subsequently recombine into a number of fragments

of various lengths and velocities (the same mixture would result from non-uniform initial spacing). The fragment drag depends on its length, i.e. number of bubbles and spacing. Compressed fragments with low spacing are faster. Trailing fragments with higher velocities collide with the slower preceding ones. On approach, the leading fragment is compressed and accelerated upwards while the trailing fragment is expanded and slowed down. The outcome of the collision depends on fragment size, collision velocity, and *Re*. The typical results are the following: merger, separation, re-pairing, and oscillation. The first three are demonstrated in Fig. 19. The interactions of bubble fragments can be very complicated, see Fig. 20. A sequence of numerous complex collisions eventually results in the long-time chain structure where the fragments are finally ordered according to their rise velocities. The free-end chain may possess a stable equilibrium solution where all bubbles rise in one piece, but the spacing cannot be uniform.

3.1.4.2. Non-local interactions. The distant effects result in progressive drag reduction down the chain until the limit drag C^{**} is reached. This drag does not depend on bubble position, and applies to the rest of the chain. The convergence is rapid so that the distant effects can influence only the first several dozen bubbles and could be important for short chains. The down-chain drag gradient generates an *additional viscous attractive force* between bubbles. This force enhances the viscous instability of pairing-off, Fig. 18, and also leads to formation of longer fragments at low *Re*. At high *Re*, the additional drag difference between fragments results in higher relative velocity that turns into a large collision force and a more broken chain structure is produced.

3.1.5. Low/high Reynolds number limit

In *low Reynolds number limit*, only the attractive viscous force (5) remains in the equations

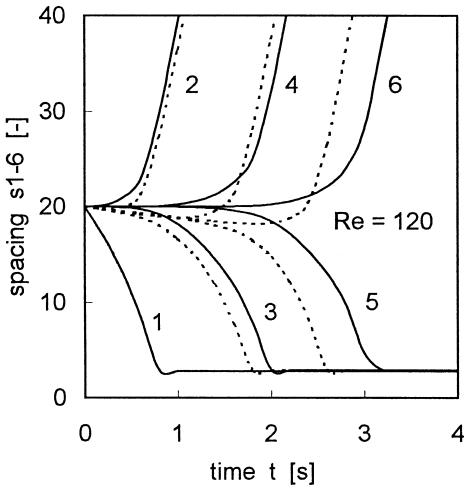

Fig. 18. Free-end chain. $N = 7$. Pairing-off. Nearest-neighbour approximation (full lines). Distant effects at $k = 0.2$ (dotted lines). Initial spacing $s_i = 20$ and velocity $v_i = 0$. Fixed-tail spacing $s_7 = 20$ ($Re = 120$).

of motion (14). Because of the absence of any repulsion, this attraction leads to physical contact between colliding particles and to coalescence in real coalescent systems. For a uniform initial spacing, pairs of touching particles gradually pair off the chain. In a chain with non-uniform spacing, closely spaced particles form clusters that condense in collisions and form even longer clusters. Non-local viscous interactions, which increase the attractive force, will enhance the tendency to aggregation.

In *high Reynolds number limit*, only the repulsive inviscid force (Eq. (8)) controls the chain

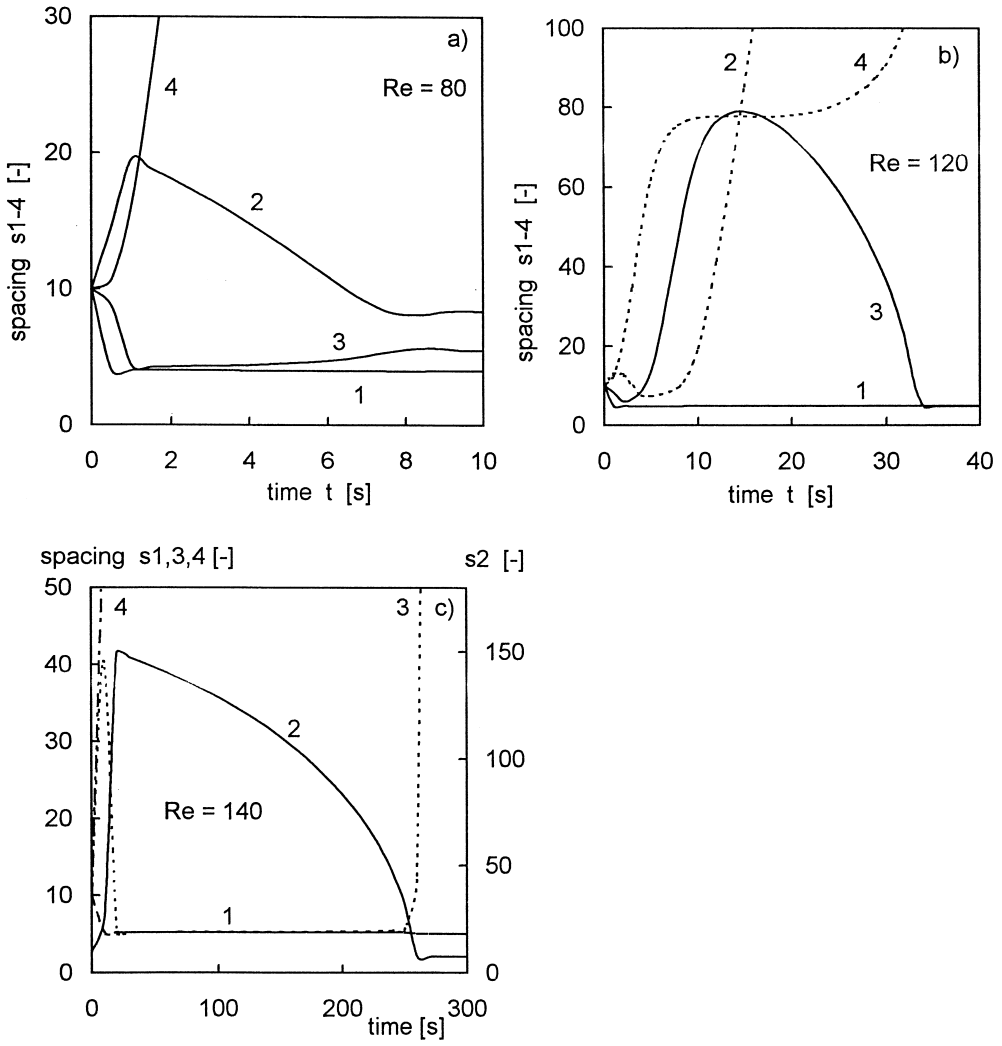

Fig. 19. Free-end chain. $N = 5$. Interaction of fragments in bubble chain. (a) Merger of two pairs after pairing-off (quadruplet 1&2&3&4 + singlet 5, s_4 diverges) ($Re = 80$), (b) separation of two pairs (doublet 1&2 + doublet 3&4 + singlet 5, $s_{2,4}$ diverge) ($Re = 120$), (c) re-pairing (triplet 1&2&3 + doublet 4&5, s_3 diverges and s_4 returns later on) ($Re = 140$).

behaviour. The chain expands unlimitedly due to the absence of any boundary. Possible non-local inviscid interactions, which increase the repulsive force, will advance the separation.

3.2. Fixed-end bubble chain

The relevant equations of motion are (14) with the fixed-end boundary condition (14c). Unlike the free-end chain, all particles here obey the same drag law (Eq. (4)) and allow for uniform spacing given by the boundary values $s_0 = s_N$. This equilibrium spacing may be either stable or unstable. Propagation of disturbances along the chain and complicated dynamics are

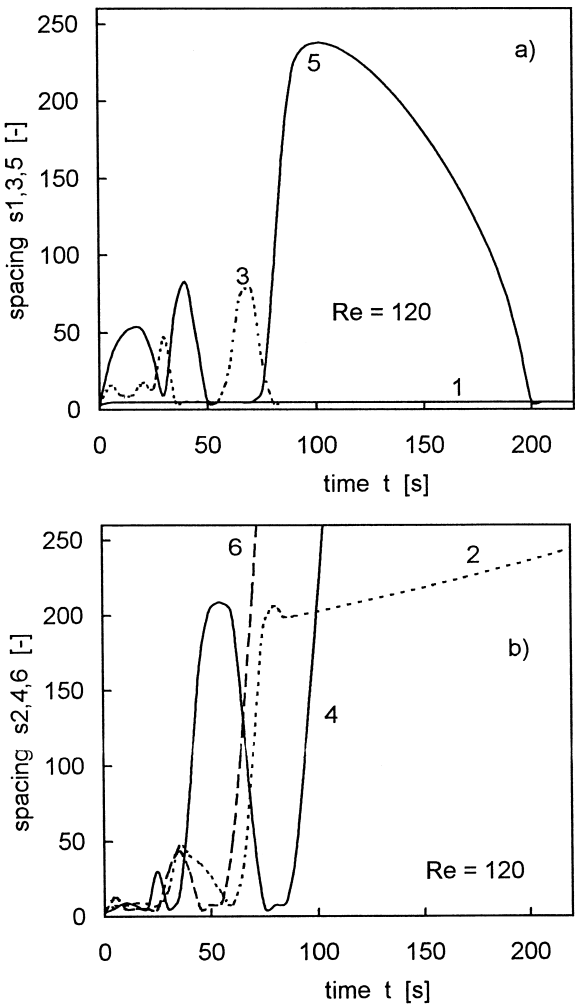

Fig. 20. Free-end chain. $N = 7$. Interaction of fragments in bubble chain. Complicated collisions finaly yield a long-time broken structure of the chain (doublet + doublet + doublet + singlet, $s_{2,\,4,\,6}$ diverge): converging spacings (a), diverging spacings (b) ($Re = 120$).

the typical features of the fixed-end chain. This kind of chain represents the hydrodynamic counterpart of the mechanical masses-on-spring system.

3.2.1. Vertical stability

Linear stability analysis shows that low uniform spacing is stable while high spacing is not. An N-bubble chain has $2N-1$ eigenvalues (N velocities and $N-1$ distances) that are both real and complex conjugated and depend on Re and s_0. N directions are always stable with eigenvalues approx. -10^1, however, $N-1$ directions become unstable approx. $+10^{-1}$ almost simultaneously at the critical values of the parameters. The eigenvalues are almost independent of the number of bubbles in the chain (calculated for 2–10 bubbles). The critical value of the spacing is shown in Fig. 21. The unstable region increases with decreasing Re. Calculations show that the instability is caused mainly by viscous effects.

1. *Local disturbances*: Deviations from uniform spacing represent concentration (density) disturbances. The departure from uniformity can be either positive (gap) or negative (compression). The evolution of disturbances depends on Re because there are two different transmission mechanisms, viscous and inviscid. The inviscid mechanism propagates a gap symmetrically to both sides. The gap is filled with the two nearest bubbles repelled from their neighbours, the original gap closes, and two new gaps are created next. The viscous mechanism consists basically in pairing-off below the gap and progresses downwards. The bubble below the gap behaves as the leading bubble in the free-end chain. Pairing-off in this context transmits a sequence of alternating compressions (spacing in pairs) and gaps (spacing between pairs). The viscous mechanism works against the inviscid one and this reduces the amplitude in the downward direction. The propagation of a local gap in a 10-bubble chain is shown in Fig. 22, where one particular distance s_5 was perturbed. The downchain amplitude (spacing 6 and more) is smaller than upchain amplitude (spacing 4 and less).
2. *Large-scale disturbances*: A spacing disturbance in a longer part of the chain mimics a

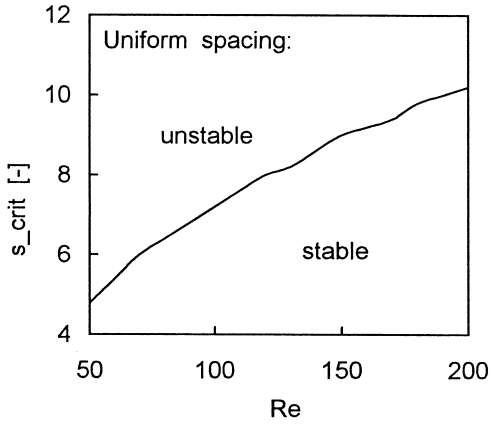

Fig. 21. Fixed-end chain. $N = 2$–10. Vertical stability of the chain. Uniform spacing is unstable at large spacing and low Reynolds number (positive real parts of eigenvalues).

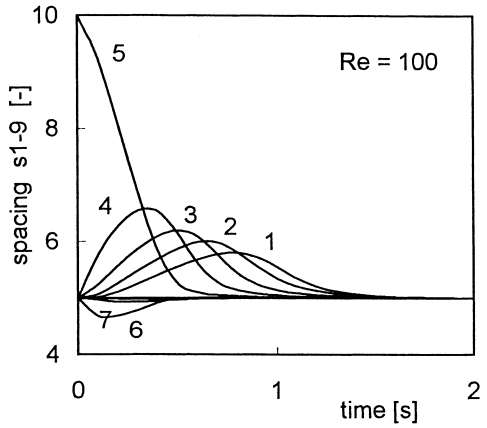

Fig. 22. Fixed-end chain. $N = 10$. Propagation of localised disturbances. Bubble chain as a transmission line. Local gap $s_5 = 10$ propagates through chain with uniform spacing $s_0 = 5$. Upchain amplitude (spacing 4, 3, 2, 1) of the travelling disturbance is larger than the downchain amplitude (spacing 6, 7, 8, 9) ($Re = 100$).

macroscopic region with higher or lower particle concentration in uniform one-dimensional medium. The chain represents a window with spacing s' within a longer chain with spacing $s_0 \neq s'$. For compression $s' < s_0$, the relaxation of s' to s_0 is quick and almost simultaneous for all bubbles. The more compressed window merely expands like a spring. For a gap, $s' > s_0$, the return is slow and proceeds subsequently from the bottom. Fig. 23 shows the closing of a large gap from below (first relaxes s_4, then s_3, etc.). Unlike bubbles rising in *general* positions, the denser parts of the *in-line* arrangement, the chain, move faster. The dense part below the gap collects the diluted bubbles along the way and tends to close the gap. The fast denser part above the gap tends to open it even more. The result depends on

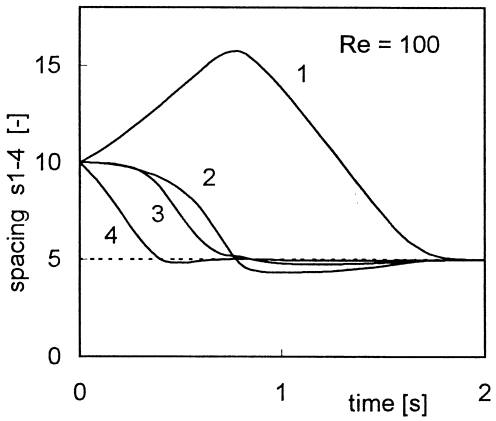

Fig. 23. Fixed-end chain. $N = 5$. Propagation of large-scale disturbances — bubble chain as the prekursor of voidage waves in real one-dimensional bubbly flows. A diluted five-particle window (large spacing $s = 10$) evolves in uniform chain with large particle concentration (low spacing $s = 5$). The window closes from below (spacing 4, 3, 2, 1) ($Re = 100$).

the size of the disturbance. For large concentration difference $s' - s_0$, the chain breaks into two parts separated by a blank region — the shock wave. In reality, the two bubbles demarcating the gap (being fixed in this model) will be repelled form the dense regions to the sparse ones by hydrodynamic diffusion making the transition gradual.

3.2.2. Vertical instability

Linear stability analysis applies only to 'small' disturbances of uniform spacing. This uniformity can be broken by either a large enough disturbance in the stable region or a small suitable disturbance in the unstable region. The chain then becomes fragmented (like the free-end chain) or the bubbles enclosed within the boundaries (unlike the free-end chain) undergo complicated behaviour.

Dissipative chaos. Interactions within the chain become complex at low *Re* where viscous effects are strong. The amplitude of travelling disturbances is higher, the relaxation is slower, and the part of the chain affected is larger. The chain dynamics changes from quick and damped relaxation, through damped and persistent oscillations, to highly irregular oscillations, commonly recognised as chaos. Fig. 24 demonstrates the gradual destabilisation of the uniform equilibrium. At low *Re*, the bubbles cannot stay in equidistant positions; they must move constantly so that they oscillate. The collective oscillations acquire irregular character, since many frequencies are mixed up. There are several signs of the chaotic signal (Schuster, 1995): the autocorrelation function decays rapidly, the power spectrum is continuous with broad noise located mostly at low frequencies, Kolmogorov entropy is a finite and positive number, and the fractal dimension of the attractor can be a non-integer number. The autocorrelation function and the spectrum of the signal (Fig. 24(f)) are shown in Fig. 25 with values of $K \approx 1.7$ (bit/s) and $D \approx 2.6$ (30,000 data points sampled by 200 Hz).

3.2.3. Chain velocity

The remarkable feature of the in-line arrangement of particles is the collective drag reduction. The lower the spacing (higher particle concentration), the higher the drag reduction and the chain velocity, see Fig. 26.

3.2.4. Non-local interaction

Like the free-end chain, the non-local interactions affect only the first several dozen bubbles until the limit drag C^{**} is reached. Unlike the free-end chain, it does not make real sense to study these first bubbles. In experiments, where the fixed-end chain means a continuous chain passing through a liquid layer, they escape at the surface. In the theoretical model, where the fixed-end chain represents a window in a longer chain, these bubbles are not the first ones. Distant interactions generate additional chain drag reduction. Fig. 26 shows the increase of chain velocity with increasing intensity of the distant coupling (calculated from Eq. (2) with non-local drag coefficients). The measurement of the chain velocity versus bubble spacing

enables the experimental determination of the strength k of the distant coupling within the chain.

3.2.5. Low/high Reynolds number limit

The presence of boundaries causes less trivial limit behaviour compared to the free-end chain. The pivot velocity is determined by spacing s_0 and is generally not the least in the chain.

In *low Reynolds number limit*, only the attractive viscous force controls the chain behaviour.

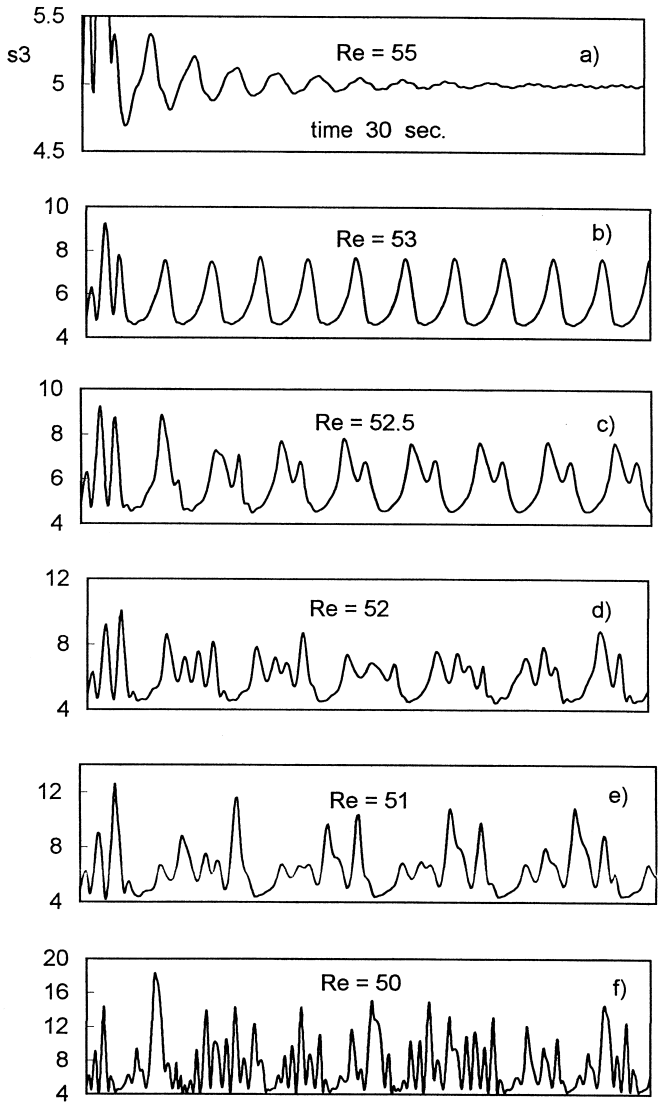

Fig. 24. Fixed-end chain. $N = 7$. Chaotic behaviour of bubbles in chain. Destabilization of the equilibrium uniform spacing by decreasing Reynolds number (a–f). Initial spacing $s_i = [5, 5, 5, 8, 5, 5]$ and velocities $v_i = 0$. Boundary spacing $s_0 = 5$.

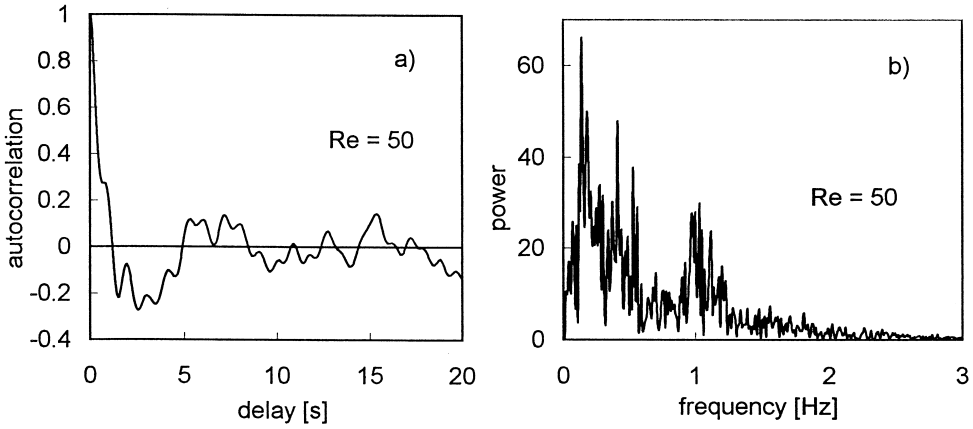

Fig. 25. Fixed-end chain. $N = 7$. Chaotic signal. (a) Autocorrelation function decays rapidly. (b) Broad-band noise appears in the power spectrum. (100 s of the signal from Fig. 24(f) sampled by 100 Hz) ($Re = 50$).

In a chain with uniform initial spacing s_i, pairing-off starts from the first bubble for $s_i < s_0$, the first bubble escapes and the pairing-off starts from the second bubble for $s_i > s_0$, and the chain occurs in an unstable equilibrium for $s_i = s_0$, which breaks into non-uniform spacing after a small perturbation. A chain with non-uniform spacing basically follows the free-end chain scenario.

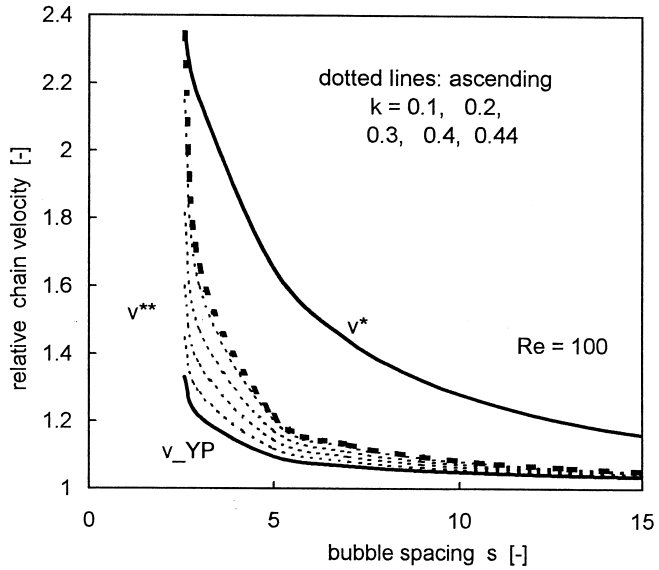

Fig. 26. Fixed-end chain. $N = \infty$. Chain rise velocity. Effect of (i) bubble spacing and (ii) distant interactions. Nearest-neighbour approximation: v_{YP} is the lower bound on the chain velocity (bottom full line). Non-local interactions (YP model): chain velocity v^{**} increases with increasing distant coupling k (dotted lines). Non-local interactions (KM model): v^* is the upper bound on the chain velocity (top full line). (Corresponding drag coefficients C_{YP}, C^{**}, and C^* are shown in Fig. 6) ($Re = 100$).

In *high Reynolds number limit*, only the repulsive inviscid force controls the chain behaviour. Uniform spacing here represents an unstable (more precisely, neutrally stable with zero eigenvalues) equilibrium of rest. The potential energy introduced into the system by deforming the equilibrium elastic 'hydrodynamic spring' converts into the kinetic energy of the particle motion. The energy flows through all possible oscillatory modes and reflects from boundaries thus remaining in the system: conservative chaos. Possible inertial distant effects are expected to affect the fine structure of the chaos.

4. Comparison with experiment

The key phenomena predicted by the model are compared with results on hydrodynamic interactions of particles in a linear array previously published in the literature. The comparison is mainly qualitative, because there are almost no experimental data available on dynamic behaviour of individual particles in a chain.

4.1. Free-end chain

1. *Two bubbles*: The model agrees well (even quantitatively) with the results obtained by the direct solution of the Navier–Stokes equation by YP, regarding both the steady solutions and the transient dynamics. This provides the validation of the model for the case of two bubbles.
2. *More bubbles*: The model predicts re-pairing as the typical phenomenon in a chain with three or more bubbles. Re-pairing was observed in a low *Re* chain of three particles, both in experiments (Happel and Pfeffer, 1960; Leichtberg et al., 1976a) and numerical simulations (Leichtberg et al., 1976a). The model predicts pairing-off as the typical phenomenon in a chain with four or more bubbles. Pairing-off was predicted theoretically (Morrison, 1973; Harper, 1983; Lerner and Harper, 1991) and numerically (Leichtberg et al., 1976a) and was observed in experiments (Leichtberg et al., 1976a, KM). The model predicts the fragmentation of the free-end chain, complex interactions between fragments, and the resulting long-time quasi-steady fragmented structure of the chain. This scenario was observed in experiments and simulations (Leichtberg et al., 1976a). The model also predicts possible persistent oscillations in a system of four bubbles in a vertical line. Oscillations of three (Caflisch et al., 1988) and four (Durlofsky et al., 1987) freely sedimenting particles starting from corners of a triangle and horizontal square were predicted. The model predicts the physical contact of bubbles in pairs (and longer clusters) in low *Re* limit, which leads to coalescence in real coalescent systems. Coalescence in bubble pairs was observed in experiments (KM).

4.2. Fixed-end chain

The model predicts the existence of uniform equilibrium spacing as the typical feature of the

fixed-end chain. Uniform steady spacing was observed in numerous experiments with chains of bubbles and drops (see Section 1). The model predicts chain drag reduction with decreasing bubble spacing. The chain drag reduction was observed in many experiments (Poutanen and Johnson, 1959; Crabtree and Bridgwater, 1969; Marks, 1973; Omran and Foster, 1977; Martin and Chandler, 1982; Li et al., 1997b, Li et al., 1998). The model predicts the existence of travelling concentration disturbances along the chain. Concentration waves in real one-dimensional bubbly flows were predicted theoretically and observed in numerous experiments (e.g. Lammers and Biesheuvel, 1996). The model predicts the complicated chaotic behaviour of bubbles at low *Re*. The chaotic dynamics was observed in experiments (Nguyen et al., 1996, Li et al., 1997a). Generally, complicated dynamics of mechanical one-dimensional arrays is well known and has been studied since Fermi–Pasta–Ulam times (e.g. Jackson, 1990).

All these predictions were obtained in the nearest-neighbour approximation. It seems that the non-local interactions may not always be strong. The intensity of these interactions expressed by k can be determined experimentally as suggested in Section 3.

When pursuing the analogy between the behaviour of different two-phase systems one should be aware of the following. The net particle acceleration given by Eq. (12) is: (applied forces/particle mass) $\sim \rho_{\text{fluid}}/\rho_{\text{particle}}$. This ratio is $\sim 10^3$ for gas bubbles in liquids, $\sim 10^0$ for drops and solids in liquids and also for bubbles endowed with added mass, and $\sim 10^{-3}$ for drops and solids in gases. Weaker fluid inertial effects are, therefore, expected for drops in gas compared to bubbles. Indeed, feeling no inertial repulsion, all trailing drops unscrupulously coalesced into the leading drop in drop chains in air at *Re* about 80 (Nguyen and Dunn-Rankin, 1992). Note that for a given system, the viscous-to-inviscid ratio of the force coefficients is $C_{\text{d}}/C_{\text{p}} \sim Re^{-1} + O(Re^{-3/2})$. Another issue is the difference due to the slip/non-slip boundary conditions. For example, two side-by-side bubbles attract each other unlimitedly (Kok, 1993a, 1993b), while two drops or solids stop at an equilibrium distance (Kim et al., 1993).

5. Conclusions

The proposed model for dynamic behaviour of bubbles rising in the one-dimensional array presents considerable simplification of this hydrodynamic problem. The very special arrangement of the particles enabled us to build up the model as a composition of several ingredients: viscous drag, added mass, inertial force, buoyancy; which are believed to play the crucial role in the particle interactions. In this approximation, the particle behaviour is described simply by the Newton force law, the set of ODEs. The hydrodynamic interactions thus decomposed are transparent and it is easy to find where the given phenomenon comes from. For instance, the analysis of the non-local coupling between distant particles would be difficult to obtain otherwise. This approach is justified partly by the reasonings underlaying the modelling concept and partly by the qualitative agreement of the model predictions with experimental results. The price for the simplicity is so far unknown and the model must be tested by fine experimental measurements and numerical solution of the fundamental equations of motion.

Acknowledgements

Very special thanks to Neale H. Thomas who taught me much during the Royal Society fellowship at the University of Birmingham, UK. Thanks to Igor Schreiber (Prague Institute of Chemical Technology) for providing the computer program CONT. Messrs. A.A. Dear and R.B. Haas (Dept. Foreign Languages, CZ Acad. Sci.) improved the English considerably. This work was supported by GACR (No. 104/98/1435) and CEC Inco-Copernicus project (No. ERB IC15-CT98-0904).

Appendix A

Two formulas were suggested to fit the dependence of drag factors F_1 and F_2 on bubble spacing s calculated by YP for three values of Re, see Table 2. To keep the expressions simple, the dependence on Re was omitted and the formulas give average values. Factor F_2 was approximated by a hyperbola

$$F_2 = k_1 + \frac{k_2}{(s - k_3)^{k_4}}, \tag{A1}$$

with the following values of parameters: $k_1 = 2.2$, $k_2 = 2.5 \pm 0.2$, $k_3 = 2$, and $k_4 = 0.6 \pm 0.05$. The correlation coefficient of the log–log plot was 0.906. The formula for F_1 is less obvious. Since the graph resembles a trajectory of heavily damped pendulum, the following expression was suggested:

Table 2
Bubble drag factors [a]

Spacing, s	Factor F_1-leading bubble			Factor F_2-trailing bubble		
	Re			Re		
	50	100	200	50	100	200
2.6	1.95	1.78	0.20	4.20	5.38	8.25
3.0	2.10	2.10	2.08	3.95	4.90	5.70
3.5	2.23	2.46	2.75	3.60	4.20	4.48
4.0	2.25	2.51	2.78	3.40	3.88	4.05
5.0	2.20	2.43	2.55	3.20	3.60	3.78
7.0	2.15	2.25	2.25	2.95	3.35	3.55
10.0	2.10	2.10	2.13	2.78	3.15	3.30
15.0	2.08	2.05	2.05	2.60	2.95	3.05
20.0	2.08	2.05	2.03	2.49	2.80	2.85
25.0	2.05			2.40	2.70	
30.0	2.05			2.35	2.60	

[a] The original numerical values of the leading F_1 and trailing F_2 drag factors of the bubble pair calculated by YP (taken from Fig. 3 in YP).

$$F_1 = k_1 + k_2\big[\exp(-k_3(s-k_4)) - k_5\exp(-k_6(s-k_7))\big], \tag{A2}$$

with the following values of parameters: $k_1 = 2.2$, $k_2 = 6$, $k_3 = 1$, $k_4 = 1.2$, $k_5 = 5$, $k_6 = 2$, and $k_7 = 1.2$. No linearisation was applied here and the best fit was made on the grounds of both the low sum of squares of deviations and the visually acceptable passage of the graph through the scatter of data. In both cases, a better fit can be obtained for individual data sets with a particular value of *Re*.

References

Batchelor, G.K., 1967. Introduction to Fluid Dynamics. Cambridge University Press, Cambridge.

Biesheuvel, A., van Wijngaarden, L., 1982. The motion of pairs of gas bubbles in perfect liquid. J. Engng. Math 16, 349–365.

Caflisch, R.E., Lim, C., Luke, J.H.C., Sangani, A.S., 1988. Periodic solution for three sedimenting spheres. Phys. Fluids 31, 3175–3179.

Chiang, C.H., Sirignano, W.A., 1993. Axisymmetric calculations of three-droplet interactions. Atomization and Sprays 3, 91–107.

Crabtree, J.R., Bridgwater, J., 1969. Chain bubbling in viscous liquids. Chem. Eng. Sci 24, 1755–1768.

Drahoš, J., Ruzicka, M.C., Pěnkavová, V. 1997. Chaotic dynamics of bubble formation in a pool of liquid. In: Giona, M., Biardi, G. (Eds.), Fractals and Chaos in Chemical Engineering. World Scientific, Singapore, pp. 398–407.

Duineveld, P.C., 1995. The rise velocity and shape of bubbles in pure water at high Reynolds number. J. Fluid Mech 292, 325–332.

Durlofsky, L., Brady, J.F., Bossis, G., 1987. Dynamic simulation of hydrodynamically interacting particles. J. Fluid Mech 180, 21–49.

Ganatos, P., Pfeffer, R., Weinbaum, S., 1978. A numerical-solution technique for three-dimensional Stokes flows, with application to the motion of strongly interacting spheres in a plane. J. Fluid Mech 84, 79–111.

Guckenheimer, J., Holmes, P., 1986. Nonlinear Oscillations, Dynamical Systems, and Bifurcations of Vector Fields. Springer, New York.

Happel, J., Brenner, H., 1990. Low Reynolds Number Hydrodynamics. Prentice-Hall, Englewood Cliffs, NJ.

Happel, J., Pfeffer, R., 1960. The motion of two spheres following each other in a viscous fluid. AIChE J 6, 129–133.

Harper, J.F., 1970. On bubbles rising in line at large Reynolds number. J. Fluid Mech 41, 751–758.

Harper, J.F., 1983. Axisymmetric Stokes flow images in spherical free surfaces with applications to rising bubbles. J. Austral. Math. Soc. Ser B 25, 217–231.

Harper, J.F., 1997. Bubbles rising in line: why is the first approximation so bad? J. Fluid Mech 351, 289–300.

Helfinstine, R.A., Dalton, C., 1974. Unsteady potential flow past a group of spheres. Comput. Fluids 2, 99–112.

Jackson, E.A., 1990. Perspectives of Nonlinear Dynamics I, II. Cambridge University Press, Cambridge.

Katz, J., Meneveau, C., 1996. Wake-induced relative motion of bubbles rising in line. Int. J. Multiphase Flow 22, 239–258.

Kim, I., Elghobashi, S., Sirignano, W.A., 1993. Three-dimensional flow over two spheres placed side by side. J. Fluid Mech 246, 465–488.

Kok, J.B.W., 1993a. Dynamics of a pair of gas bubbles moving through liquid. Part I: Theory. Eur. J. Mech B12, 515–540.

Kok, J.B.W., 1993b. Dynamics of a pair of gas bubbles moving through liquid. Part II: Experiment. Eur. J. Mech B12, 541–560.

Kumaran, V., Koch, D.L., 1993a. The effect of hydrodynamic interactions on the average properties of a bidisperse suspension of high Reynolds number, low Weber number bubbles. Phys. Fluids A 5, 1123–1134.

Kumaran, V., Koch, D.L., 1993b. The rate of coalescence in a suspension of high Reynolds number, low Weber number bubbles. Phys. Fluids A5, 1135–1140.

Lamb, H., 1932. Hydrodynamics. Cambridge University Press, Cambridge.
Lammers, J.H., Biesheuvel, A., 1996. Concentration waves and the instability of bubbly flows. J. Fluid Mech 328, 67–93.
Lee, K.C., 1979. Aerodynamic interaction between two spheres at Reynolds number around 10^4. Aeronaut. Q 30, 371–385.
Leichtberg, S., Pfeffer, R., Weinbaum, S., 1976a. A study of unsteady forces at low Reynolds number: a strong interaction theory for the coaxial settling of three or more spheres. Phil. Trans. Roy. Soc A282, 585–610.
Leichtberg, S., Pfeffer, R., Weinbaum, R., 1976b. Stokes flow past finite coaxial clusters of spheres in a circular cylinder. Int. J. Multiphase Flow 3, 147–169.
Lerner, L., Harper, J.F., 1991. Stokes flow past a pair of stagnant-cap bubbles. J. Fluid Mech 232, 167–190.
Li, H.Z., Mouline, Y., Choplin, L., Midoux, N., 1997a. Chaotic bubble coalescence in non-Newtonian fluids. Int. J. Multiphase Flow 23, 713–723.
Li, H.Z., Mouline, Y., Choplin, L., Midoux, N., 1997b. Rheological simulation of in-line bubble interactions. AIChE J 43, 265–267.
Li, H.Z., Mouline, Y., Funfschilling, D., Marchal, P., Choplin, L., Midoux, N., 1998. Evidence for in-line bubble interactions in non-Newtonian fluids. Chem. Eng. Sci 53, 2219–2230.
Liang, S.C., Hong, T., Fan, L.S., 1996. Effect of particle arrangements on the drag force of a particle in the intermediate flow regime. Int. J. Multiphase Flow 22, 285–306.
Marek, M., Schreiber, I., 1995. Chaotic Behaviour of Deterministic Dissipative Systems. Cambridge University Press, Cambridge.
Marks, C.H., 1973. Measurement of the terminal velocity of bubbles rising in a chain. J. Fluid Eng 2, 17–22.
Martin, W.W., Chandler, G.M., 1982. The local measurements of the size and velocity of bubbles rising in liquids. Appl. Sci. Res 38, 239–246.
Maxworthy, T., Gnann, C., Kurten, M., Durst, F., 1996. Experiments on the rise of air bubbles in clean viscous liquids. J. Fluid Mech 321, 421–441.
Michael, P., 1965. Ideal flow along a row of spheres. Phys. Fluids 8, 1263–1266.
Milne-Thomson, L.M., 1995. Theoretical Hydrodynamics. Dover, New York.
Mittoni, L.J., Schwarz, M.P., LaNauze, R.D., 1995. Deterministic chaos in the gas inlet pressure of gas–liquid bubbling systems. Phys. Fluids 7, 891–893.
Moore, D.W., 1963. The boundary layer on a spherical gas bubble. J. Fluid Mech 16, 161–176.
Morrison, F.A., 1973. Breakup of a bubble chain. Chem. Eng. Sci 28, 1115–1116.
Nguyen, K., Daw, C.S., Chakka, P., Cheng, M., Bruns, D.D., Finney, C.E.A., Kennel, M.B., 1996. Spatio-temporal dynamics in a train of rising bubbles. Chem. Eng. J 65, 191–197.
Nguyen, Q.V., Dunn-Rankin, D., 1992. Experiments examining drag in linear droplet packets. Exp. Fluids 12, 157–165.
Omran, N.M., Foster, P.J., 1977. The terminal velocity of a chain of drops or bubbles in a liquid. Trans. Instn. Chem. Eng. 55, 171–177.
Poutanen, A.A., Johnson, A.I., 1959. Studies of bubble formation and rise. Can. J. Chem. Eng 37, 93–101.
Press, W.H., Flannery, B.P., Teukolsky, S.A., Vetterling, W.T., 1986. Numerical Recipes. Cambridge University Press, New York.
Pruppacher, H.R., Klett, J.D., 1978. Microphysics of Clouds and Precipitation. Reidel, Dordrecht.
Ramachandran, R.S., Wang, T.Y., Kleinstreuer, C., Chiang, H., 1991. Laminar flow past three closely spaced monodisperse spheres or nonevaporating drops. AIAA J 29, 43–51.
Rushton, E., Davies, G.A., 1978. The slow motion of two spherical particles along their line of centres. Int. J. Multiphase Flow 4, 357–381.
Ruzicka, M.C., Drahoš, J., Zahradník, J., Thomas, N.H., 1997. Intermittent transition from bubbling to jetting regime in gas–liquid two phase flows. Int. J. Multiphase Flow 23, 671–682.
Schouten, J.C., van den Bleek, C.M., 1996. RRCHAOS: An Interactive Software Package for Deterministic Chaos Analysis of Non-linear Time Series. Reactor Research Foundation, Delft University of Technology, Delft, The Netherlands.
Schuster, H.G., 1995. Deterministic Chaos: An Introduction. VCH Press, Weinheim, Germany.
Sirignano, W.A., 1993. Fluid dynamics of sprays. J. Fluids Eng 115, 345–378.

Tal, R., Lee, D.N., Sirignano, W.A., 1983. Hydrodynamics and heat in sphere assemblages — cylindrical cell models. Int. J. Heat Mass Transfer 26, 1265–1273.

Temkin, S., Ecker, G.Z., 1989. Droplet pair interactions in a shock-wave flow field. J. Fluid Mech 202, 467–497.

Tritton, D.J., Egdell, C., 1993. Chaotic bubbling. Phys. Fluids A5, 503–505.

Tsai, J.S., Sterling, A.M., 1990. The application of an embedded grid to the solution of heat and momentum transfer for spheres in a linear array. Int. J. Heat Mass Transfer 33, 2491–2502.

Tsuji, Y., Morikawa, Y., Terashima, K., 1982. Fluid-dynamic interaction between two spheres. Int. J. Multiphase Flow 8, 71–82.

Wang, B.X., Liu, T., 1992. Research on hydrodynamics and heat transfer for fluid flow around heating spheres in tandem. Int. J. Heat Mass Transfer 35, 307–317.

Wang, H., Skalak, R., 1969. Viscous flow in a cylindrical tube containing a line of spherical particles. J. Fluid Mech 38, 75–96.

van Wijngaarden, L., 1993. The mean rise velocity of pairwise-interacting bubbles in liquid. J. Fluid Mech 251, 55–78.

Wolfram, S., 1996. The Mathematica Book, 3rd ed. Cambridge University Press, New York.

Yuan, H., Prosperetti, A., 1994. On the in-line motion of two spherical bubbles in a viscous fluid. J. Fluid Mech 278, 325–349.

Zhu, C., Liang, S.C., Fan, L.S., 1994. Particle wake effects on the drag force of an interactive particle. Int. J. Multiphase Flow 20, 117–129.